CLM - P 2

CLM - P 2

United Kingdom Atomic Energy Authority

RESEARCH GROUP

Preprint

ENERGY LOSS PROCESSES IN ZETA

A. GIBSON D. W. MASON

Culham Laboratory,

Culham, Abingdon, Berks.

1961

U.D.C.
621.039.616.2

UNCLASSIFIED
(Approved for publication)

CLM - P2

ENERGY LOSS PROCESSES IN ZETA

by

A. GIBSON and D. W. MASON

Submitted to the Proceedings

of the Physical Society

U.K.A.E.A. Research Group,
Culham Laboratory,
CULHAM, Abingdon.
Berks.

July, 1961.

HL61/3486 (C.18)
E/F

ENERGY LOSS PROCESSES IN ZETA

by

A. GIBSON and D.W. MASON

Atomic Energy Research Establishment, Harwell, England.

ABSTRACT

The energy lost from ZETA discharges, in deuterium and argon by radiation, plasma particles and non-thermal electrons, has been investigated experimentally over a wide range of conditions. Two definite regimes of energy loss have been established. These regimes are determined principally by the pressure at which the machine is operated. At high pressures (5 microns) line radiation from impurities is the dominant loss process and under certain discharge conditions accounts for all the energy fed into the discharge. Theoretical considerations are presented to show that the observed impurity content of 10^{11} atoms/cc can account for the radiation loss. At lower pressures (0.5 microns) the energy is lost by particles, firstly by plasma which is not efficiently confined and secondly by fast electrons which are accelerated at the termination of the current pulse and strike the tube walls with about 8 keV of energy.

The results reported are related to energy loss observations made by workers with other stabilized pinch devices.

CONTENTS

ILLUSTRATIONS

TABLES

§1. Introduction

1.1 Previous Work

A number of experiments, (Allibone et al 1958; Butt et al 1958; Colgate et al 1958; Conner et al 1958; Dolgor-Savelier et al 1958.) carried out using stabilized pinch discharges to produce high temperature plasmas were described at the Geneva Conference held in 1958. In all these experiments it was evident that only a small part of the energy supplied was needed to heat the plasma to the observed temperatures and that a major part was transferred to the walls of the containing vessel. This rate of loss of energy from the plasma was in all cases very large, from 10^4 to 10^6 times the bremsstrahlung rate to be expected at the lowest operating pressures.

At the Geneva Conference, Colgate et al (1958) suggested that all the energy loss from the first half cycle of the "Gamma pinch" discharge could be due to non-thermal electrons with energies of about 2 keV: The preliminary results of M.F. Harrison (Harding et al 1958) suggested that not more than 10% of the energy loss from Zeta, at a starting pressure of 1/8 micron, was due to radiation. Energy loss by escape of plasma due to instabilities was an obvious possibility in many devices but was not demonstrated experimentally.

Since the Geneva Conference, Karr (Karr et al 1961) has shown that the energy loss in perhapsatron S4 is in many cases due principly to line radiation, although conditions can be found where this is not so. Kirillov (1960) has described a non-pinching discharge with electrodes, in a strong longitudinal magnetic field, and has shown this discharge to be essentially radiation cooled. Bernstein and Krauz (1959) have demonstrated conditions in the B-1 stellerator where plasma loss across lines of force is an important process.

This paper reports observations which clarify the energy loss position in Zeta, and by showing that different processes are important under different discharge conditions, makes it possible to understand why different groups observe differing loss processes. An outline of some preliminary results has been briefly reported at an American Physical Society Meeting (Gibson et al 1960).

1.2 The Zeta Apparatus

Zeta has been described fully elsewhere (Butt et al 1958; Mitchell et al 1959). The original 1600 μf capacitor bank has been replaced by one of 0.011f capacity

and the axial stabilizing field available has been increased to nearly 2000 gauss. These modifications enable the machine to operate at increased gas currents.

The more important parameters of the machine as used in the present work are

Bore of stainless steel liner	97 cms.
Aspect ratio	3:1
Turns ratio	4:1
Stored Energy	3 MJ at 24 kV.
Stabilizing field	160 gauss to 2000 gauss
Rise time to peak current	1 msec, pulse length (clamped) 3 msec.

For most of the experiments described in this paper the following operating conditions have been chosen:

Capacitor bank voltage 5 KV - 10 KV

Operating pressure (deuterium) $\frac{1}{2}$ micron - 10 microns

Operating pressure (argon) $^1/16$ micron - 5 microns

For these conditions the energy dissipated in the plasma has been measured by evaluating $\int V_L \times I_G . dt$ electronically (V_L = voltage round liner I_G = gas current.)

The percentage of the initial stored energy that is dissipated in the plasma depends on the discharge resistance but is typically in the region of 50%, falling to a minimum value of 30% at $1\frac{1}{2}$ micron initial pressure. The balance of the energy is dissipated in the external circuit and in the stainless steel liner.

1.3 The energy loss problem on Zeta

The energy fed into the Zeta discharge is shown as a function of time in fig. 1 together with the estimated magnetic, ionization and thermal energies. The magnetic energies in the diagram have been obtained from magnetic probe measurements made by Lees and Rusbridge (1959) and the thermal energies by assuming, at $\frac{1}{2}$ micron pressure a mean particle energy equivalent to 2×10^6 °K, and at 5 micron pressure equal ion and electron temperatures of 2×10^5 °K.

The principle difference between the low and high pressure cases is that at low pressures the inductive energy is greater due to the larger current (smaller resistance) and also at low pressures there is a catastrophic discontinuity in the gas current and hence in stored magnetic energy.

The discontinuity is accompanied by an increase in the energy fed into the discharge, this energy is that released from the external leakage inductance. Fig. 1 shows that after the first 0.5 msec a large energy discrepancy appears, and processes must exist to transport this energy to the walls of the discharge tube. We have investigated the three processes which seem most likely to contribute significantly to the energy loss, they are: loss by radiation; loss by low energy electrons (thermal to 2 keV), as plasma; and loss by electrons energetic enough to produce detectable X-rays.+

+ Magnetic field fluctuations, produced by variations of current density in the discharge may in principle gave rise to eddy current energy losses in the liner and torus walls. Estimates of these losses, based on the magnitude and frequency of the fluctuations observed (Lees and Rusbridge 1961) are, at most, a few percent of the total energy input.

§2. Energy Loss due to Radiation

2.1 Apparatus

The apparatus used (fig. 2) consists of a radiation thermopile having a nominal sensitivity of 60 mV/w/cm^2. The sensitive surface of the thermopile was coated with zinc black in order to give it a uniform response from approximately 10^{-4} microns to 20 microns. The thermocouple foil becomes transparent to X-rays above about 10 keV, and this provides the short wavelength limit of sensitivity. The long wavelength limit is probably an under estimate since absorption measurements of metallic blacks have not been made at longer wavelengths, whereas the absorption is typically greater than 80% at 20 microns. That no appreciable amount of energy is radiated outside the interval 10^{-4} - 20 microns is shown by X-ray (see §3) and infra red (Harding et al 1961) observations. Microwave observations by A.N. Dellis at 4 mm (Dellis 1961) and 8 mm (Harding et al 1958) reveal no emission grossly more intense than the negligible thermal radiation.

The output of the thermopile was displayed on a critically damped galvanometer; the response time of the complete system was 1 sec so that an integrated signal was obtained, because of the long time constant and low impedance there was no difficulty due to electrical interference. The sensitivity of the system was such that it could readily measure radiation from a uniform channel 50 cms in diameter when the energy radiated was about 1% of the capacitor bank energy, the accuracy of the galvanometer readings was typically $\pm$ 5%.

2.2 Calibration

The thermopile was calibrated in vacuum against a standard tungsten lamp, the radiation from the lamp was pulsed by means of a rotating slotted disc. In order to obtain a large enough signal a 35 msec pulse was used and it has been verified that the response was a linear function of pulse duration down to 5 msec, the duration of the ZETA pulse. Three pulse calibrations were made over a period of 6 months or so and the calibration was reproducible to better than 3%.

2.3 Geometry

In order to pass from the energy incident on the thermopile to the energy radiated by the discharge, it is necessary to know the geometry of the radiating channel. Thus for a given amount of energy falling on the thermopile

6.5 times more energy would be radiated, in total, by a uniform source filling the discharge tube than by a line source on its axis.

We have estimated the radiation geometry by taking pinhole photographs of the discharge looking both horizontally and vertically. The photographs were recorded on a photographic plate in contact with a sodium salycilate screen. A sodium salycilate phosphor has a uniform quantum efficiency over a wide range of wavelengths (Watambe and Inn 1953), this means that in terms of energy, distributions from the pinhole camera will be weighted in favour of the long wavelengths. To offset this effect filters of aluminium and indium were inserted between the pinhole and the screen. We have found (see §2.4) that an appreciable part of the radiation from deuterium discharges lies within the transmission windows of both indium and aluminium, distributions measured through these filters were essentially the same. A large part of the radiation from Argon discharges lies within the indium window but much less lies within the aluminium window, accordingly measurements for this gas were made through indium filters.

The photographs obtained in this way were photometered and converted to intensities incident on the plate by using the measured characteristic of the plate. These intensity distributions were compared with the distribution to be expected on the photographic plate from various combinations of uniform radiation sources of different radii.

Pinhole photographs taken in the horizontal plane showed an ~~in~~ward displacement of the radiating channel of about 10 cms. No correction to the geometry factors has been applied to take account of this shift but the correction is less than 10%. No vertical displacement was observed. Since the angle of view of the thermopile is small no correction need be applied for the toroidal shape of the discharge.

The ratio of the geometry factor obtained from the fitted uniform source to that for a line source on the axis is given in Table I. The error in the geometry factor arising from curve fitting is of the order of 10% and the factors are reproducible to this error over long periods of time (three months).

TABLE I

Gas	p microns	Bz Gauss	KV	Ratio of distributed to line source geometry factor
D_2	$\frac{1}{2}$	150	10	3.6
D_2	$\frac{1}{2}$	375	10	4.0
D_2	1	375	10	3.3
D_2	2	375	10	2.5
D_2	4	375	10	2.5
D_2	5	750	10	2.7
D_2	6	900	15	2.7
D_2	8	375	10	2.5
A	$\frac{1}{2}$	750	10	2.9
A	2	750	10	3.4
A	2	375	10	3.4

It will be noticed from Table I that the geometry factor is not sensitive to Bz field; for this reason the same geometry factor has been used for all conditions at the same pressure and has been taken as 2.5 at all pressures above 2 microns in deuterium and as 3.4 at all pressures above 2 microns in Argon. These results are derived on the assumption that the source is a transparent radiating body; a surface radiator of the same diameter would be experimentally difficult to distinguish. Such a surface source would arise in the case when complete self absorption occurs and in this limit the geometry factor should be increased to twice the transparent source value.

2.4 Results

Measurements of radiation energy loss have been made for discharges in deuterium and argon and in deuterium with added impurities. Shot to shot variation in thermopile output was typically 10% of the mean value for any one discharge condition. The values given here are averages of ten shots.

Deuterium

The radiation emitted by a deuterium discharge in Zeta varies from a few percent to 100% of the energy input depending on the operating conditions. The variation of radiation loss with pressure and capacitor bank voltage is shown in fig. 3.

Variation with pressure

The most striking feature of the curves is the rapid increase of radiation between 1 micron and 5 microns pressure. The general form of the curves and the pressure at which the increase begins are reproducible, but the precise pressure at which the maxima occur and the absolute intensity of radiation are subject to some variation. Depending on the degree of impurity in the discharge variations of 25% in the intensity and of a factor of two in the pressure for maximum radiation have been observed.

Variation with energy input

Discharges for which the stored capacitor bank energy exceeds 1 MJ (15 kV) show that at high pressures radiation losses account for the total energy input. The two curves obtained at lower capacitor bank voltages (5 kV and 10 kV) exhibit maxima. In view of the uncertainty in the geometry of the radiating channel at these high pressures due to the possibility of self absorption, controlled amounts of impurity were added on the assumption that, if the plasma was in fact radiation cooled and the geometrical factor used was incorrect, the addition of extra impurity to the discharge should produce no observable effect. The results of these experiments showed that the radiation detected increased at first as the impurity content was raised but reached a saturation value, independent of the impurity ion added (methane, argon and nitrogen were used). This level was approximately twice that obtained with no impurity added. The saturation value was close to that obtained in pure argon discharges under the same conditions. Finally the impurity input was cut off but the radiation level remained unchanged, extensive discharge cleaning of the torus being required to produce the original lower radiation level. The saturation level observed is therefore, independent of the initial distribution of impurity i.e. it may be distributed through the discharge volume as gas or on the liner as surface contamination. This result suggests that the same geometry factor should be used for both contaminated and uncontaminated discharges since in the latter case the liner is the only source of impurity. If this assumption is correct then the maxima in the radiation curves, observed under clean conditions, represent real maxima in the radiation energy loss under these conditions.

Variation with Stabilising Field (Bz)

At high pressures the radiation losses were, within the experimental accuracy, independent of the magnitude of the stabilising field.

At low pressures however, the radiation loss increased as the stabilising field was reduced. Thus a threefold increase in radiation was observed as θ varied from one to five (θ is defined as maximum pinch field at the liner divided by the initial stabilising field at the liner). A similar dependence has been observed for the rate of impurity injection into the plasma (Burton and Wilson 1961).

Argon discharges

The variation in radiated energy with pressure is shown in Fig. 4 for two conditions in argon. The radiation shows a similar increase with pressure to that observed in deuterium but over a much lower pressure range, 0.05 - 0.25 microns compared with 1-5 microns in deuterium. At pressures greater than 0.25 microns argon discharges are essentially radiation cooled, although some decrease in radiation with pressure is observed especially at low energy input, this behaviour is similar to that in deuterium.

The results shown in fig. 4 are in some cases in excess of 100% of the energy input; this is probably due to the errors involved in estimating the radiation geometry.

Observations of the energy radiated from deuterium plasmas with small percentages of argon added as an impurity show that as the operating pressure is raised from $\frac{1}{2}$ to 6 microns the percentage of argon required to produce a radiation cooled plasma decreases from about 15% to below 5%. The result is of course to be expected as the excitation rate of the Argon ions varies as n_e, the electron density.

Spectral Range of the Radiation

Measurements made with various filters give some indication of the spectral range in which radiation is emitted. Approximately 5% of the radiation from deuterium discharges at $\frac{1}{2}$ and 5 micron pressures was transmitted by a sample of fluorite 1.3 mm thick. The transmission of the sample was measured to be 10% at 1490 Å and 25% at 1650 Å, this indicates that the bulk of the radiation is emitted at wavelengths shorter than 1600 Å, although

it is still possible for 30% of the radiated energy to be due to the CIV resonance line at 1550 Å. The transmission of indium and aluminium films was also observed, the aluminium films, 1000 Å thick had a transmission which decreased approximately linearly from 75% at 180 Å to zero at 800 Å [f], the indium films 3000 Å thick had a peak transmission of 6% at 790 Å and a mean transmission of 3% in the range 760 to 960 Å. At 2 micron pressure the aluminium filters transmitted 12% of the radiation from a deuterium discharge and the indium filters 4%, this suggests most of the radiation is in the 600 — 1000 Å range. Both filters transmitted 4% of the radiation from Argon discharges at pressure greater than $\frac{1}{2}$ micron suggesting that the radiation here is in the 800 to 1000 Å range.

2.5 Effect of particle bombardment

Since thermocouples are sensitive to particle bombardment the results obtained represent an upper limit to the energy loss by radiation. However, the transverse magnetic field in the narrow bore tube in front of the thermopile serves as a screen against plasma since the field lines are terminated on the walls of the aperture tube and probe port. For the minimum magnetic field of 160 gauss at the thermopile the velocity of plasma across the field lines is calculated to be less than one per cent of ion thermal speed. (Spitzer 1956). The tube is five diameters long and a lower limit for the attenuation of the plasma may be obtained by ignoring the diffusion (but not collisionless streaming) of plasma along the field lines. This results in an attenuation of at least five hundred and this is clearly a gross underestimate. This plasma represents a negligible energy flux to the thermopile.

Neutral particles are unaffected by the magnetic field and may in principle contribute to the signal observed. However, the filter measurements described in section 2.4 are inconsistent with the assumption of a large contribution from energy sources other than ultraviolet radiation.

2.6 Comparison of the observed radiation intensity with that calculated for impurity radiation from a low density hydrogen plasma

The dominant processes controlling the emission of spectral lines in

---

[f] The transmission of the aluminium filter was measured by G. Freeman of the University of Reading.

a low density plasma are excitation by electron collision, followed by radiative decay. The number of excitations of a particular ion species per cc per second in a thermal plasma with electron temperature Te, electron density n_e/cc and density of ion species n_i/cc can be written:

$$n_e n_i S(T_e) . \qquad (1)$$

Woolley and Stibbs (1953) give a semi-classical expression for the rate coefficient $S(T_e)$ for excitations to a level with oscillator strength f and excitation potential χ

$$S(T_e) = f/\chi \left[\frac{12\pi e^4}{2\pi m k T_e}\right]^{1/2} \Lambda \qquad (2)$$

$$\Lambda : e^{-x}\left\{1 - x e^{x} E_1(x)\right\}$$

where $x = \chi/kT_e$ and $E_1(x) = \int_x^{\infty} \frac{e^{-x}}{x}\, dx$

In view of the method of excitation most of the strongly radiating lines in Zeta will have x of the order of and less than unity. When x varies from 0.1 to 1.0, Λ varies from 0.8 to 0.2 so we shall not be in error by more than a factor 2 if we set $\Lambda = 0.4$. With this value for Λ and setting f = 1, as will be the case for strong resonance lines, we can deduce from (1) and (2) an expression for the power radiated by the plasma:-

$$P = \frac{10^{-24} n_e n_i}{(kT_e)^{\frac{1}{2}}} \quad \text{WATTS/CC} \qquad (3)$$

where n_i is now the total number density of radiating impurity ions and (kTe) is in electron volts. The expression (3) would not be changed by more than a factor 2 if the Born approximation expressions for the excitation cross section derived by Seaton (Allen 1960) or Knorr (1958) had been used. The expression represents a lower limit to the radiation in that it is assumed that there is only one strong line for each ion.

Equation (1) will not be applicable at high densities, in particular it will not apply at densities where radiation trapping or stepwise excitation have become important. McWhirter (1960) has shown that these processes are not important provided:

$$n_e < 5\times10^{12}\chi^3(kT_e)^{1/2}e^{-\chi/kT_e}$$ (stepwise excitation)

and $$n_i D < 10^{11}\chi(kT_i)^{1/2}$$ (radiation trapping)

where: D = dimension in line of sight (plasma diameter)

(kT) is in eV χ = excitation potential in eV.

In Zeta only the second condition is important and for $\chi \sim kT_i \sim 20$ eV becomes:

$$n_i < 2\times10^{11}/cc \quad \ldots\ldots (4)$$

Table II compares the observed radiation levels with those calculated from equation (3) with an impurity ion density $n_i = 10^{11}/cc$, the calculated values include the effect of a 2:1 radial compression of the plasma.

TABLE II

p microns	Assumed (kTe) eV	n_e/cc	W calc. Joules 3 msec pulse	W.obs Joules Vc = 10 kV
$\frac{1}{2}$	36	3.5×10^{13}	5.2×10^{4}	2.3×10^{4}
1	25	7×10^{13}	12.6×10^{4}	2.7×10^{4}
2	16	1.4×10^{14}	3.4×10^{5}	0.9×10^{5}
4	9	2.8×10^{14}	8.4×10^{5}	1.8×10^{5}
8	4	5.6×10^{14}	2.6×10^{6}	1.8×10^{5}

Griffin (1961) has estimated the amount of oxygen and nitrogen impurity, present in nominally clean conditions in Zeta at 1 micron pressure, to be about 10^{11} oxygen and nitrogen atoms/cc. It is likely that similar amounts of other impurities are present, although, of course, not all these atoms will be present as ions which can radiate strongly. Table II shows that an amount of impurity comparable with that detected experimentally can easily produce enough line radiation to account for all the radiation emitted by the plasma. Table II also shows that the observed increase in radiation with pressure can be accounted for by the increase in electron density alone taking a constant impurity content. Spectroscopic observation (W.M. Burton 1960) of the light from the dominant impurities carbon, nitrogen and oxygen show that this light has a similar behaviour with pressure to the observed total radiation, a numerical comparison is not possible because an intensity calibration is not available for the spectrograph.

§3. Energy Loss by Thermal Particles

The direct measurement of the energy transferred to the walls by thermal particles is difficult. Ideally one should measure the quantity:

$$\Sigma \int A.n.E.v_{\perp}.dt$$

where $A.n.v_{\perp}$ is the particle flux to the wall and E is the energy of the particles - the summation being taken over both ions and electrons.

We have attempted the considerably easier task of measuring the energy and density of one specie of particle - electrons - at the wall, and estimating the energy lost from the plasma by such particles.

It has proved possible, by the technique described below to show that for those discharge conditions for which energy losses by radiation are relatively small, the electron density at the wall is high ($> 10^{13}$/cc) and that these electrons have an energy distribution (see section 3.4) consistent with their being constituents of a plasma rather than photo-electrons emitted from the probe or liner system.

At higher pressures, where radiation dominates the energy loss, the detected electrons have energies of a few electron volts only and are therefore indistinguishable from photo-electrons emitted from the liner and probe.

3.1 Electron detection and energy analysis

One cannot readily obtain consistent data from conventional Langmuir probes in Zeta at pressures below a few microns. For this reason the probe described in this section has been developed and is shown diagrammatically in Fig. 5. It consists essentially of an energy analysing grid g_2 followed by an electron scintillation counter. The grid system is enclosed in a 7.5 cm. diameter tube having a flat on one side, in which is a pinhole aperture. The probe is pumped to about 5×10^{-5} mm mercury to prevent electrical breakdown between the grids. The tube is at liner potential and the pinhole disc is insulated from it. Grid g_1 is biased positive with respect to the pinhole aperture and serves to prevent ions reaching g_2 with the possible generation of secondary electrons. The analysing potential is applied between the pinhole disc and g_2. The remaining grid g_3 is connected to the aluminised surface of the phosphor. Electrons with sufficient energy to overcome the potential difference between g_2 and the pinhole disc are accelerated by the four kilovolts

bias applied between g_2 and g_3 and are detected by the scintillator. Field penetration through the grid system limits the energy resolution to about 4 eV.

A transistored gated integrator measures the output of the photomultiplier. On Zeta gate widths of 500-750 μ sec were generally used and most results given below were obtained with the gate centred on peak gas current.

In many cases the electron current to the scintillator phosphor is large enough to be measured directly. The phosphor is then used as a collector electrode, the current passed through a 100 ohm load resistance, this resistance being the input impedance of the gated integrator. For this mode of operation the phosphor is biased 300 + ve with respect to g_2 and the field penetration is less serious, permitting energy resolution to about 1 electron volt.

Only electrons travelling along magnetic field lines which, passing through the pinhole, intersect the phosphor, can be detected. The probe construction limits the acceptance angle to 60°. The device may be rotated about its axis so that magnetic field vector at the wall lies within the acceptance angle for any chosen interval of the current pulse.

3.2 Calibration

The probe has been calibrated by replacing the pinhole by a 1 mm aperture and focussing a beam of electrons on to it. The current of electrons to the phosphor was measured by observing the voltage drop across a load resistance in the phosphor E.H.T. supply. In this way the gated integrator output was compared directly with the total charge received by the phosphor.

3.3 Derivation of n_e and T_e from Probe Results

To obtain electron densities from the probe described here a number of simplifying assumptions have been made. The simplest treatment provides a method of calculating a lower limit for n_e with some confidence and a reasonable correction to this gives a result which is in good agreement with that obtained by microwave reflection techniques.

We first consider a Maxwellian distribution of electrons in the region of the probe and calculate the probe signal to be expected assuming the ions have no effect. The distribution function expressed in terms of the component of

velocity, $v_{\parallel}$, parallel to the magnetic field is

$$n_{\parallel}(v_{\parallel})\, dv_{\parallel} = X . e^{-\frac{m v_{\parallel}^2}{2kT}} . dv_{\parallel}$$

where $n_{\parallel}(v_{\parallel})$ is the number of electrons/cc with component of velocity between $v_{\parallel}$, $v_{\parallel} + dv_{\parallel}$ and X is a function of the electron density only.

The rate at which electrons stream along the field in one direction is:

$$n_{\parallel}(v_{\parallel}) . v_{\parallel} . dv_{\parallel} = X . v_{\parallel} . e^{-\frac{m v_{\parallel}^2}{2kT}} . dv_{\parallel}$$

If we assume that the above expression represents the current density through the pinhole, then the number of electrons arriving at the phosphor when there are V volts on g_2 is given by:

$$S_n = X . \pi . r^2 . \int_{v_{CRIT.}}^{\infty} v_{\parallel} . e^{-\frac{m v_{\parallel}^2}{2kT}} . dv_{\parallel} = X . \pi r^2 . \frac{kT}{m} . e^{-\frac{eV}{kT}} \quad (5)$$

where πr^2 is the area of the pinhole and $v_{CRIT.} = \left(\frac{2eV}{m}\right)^{\frac{1}{2}}$

hence a plot of log S_n against V is a straight line with gradient equal to $-\frac{eV}{kT}$ (6) . With $V = 0$ the total electron flux through the pinhole is

$$I_{MAX} = \frac{n_e . \bar{v}_{\parallel} . \pi r^2}{4} \quad (7)$$

where $\bar{v}_{\parallel} = 2.\left(\frac{2kT}{\pi m}\right)^{\frac{1}{2}}$

Thus we may measure n_e and T_e at the probe. There are four assumptions implicit in the above treatment:

These points are discussed below:

(1) The pinhole aperture is infinitely thin.

(2) There are no space charge effects within the probe.

(3) There are no sheath potentials associated with the probe plasma interface.

(4) That the probe does not modify the plasma.

The pinhole is 0.005" in diameter. The material from which it is made (molybdenum) is 0.0007" in the pinhole region. Thus the aspect ratio of the pinhole is approximately 7 to 1. In general only those electrons with $v_{\perp}$ large compared with $v_{\parallel}$ and which enter the pinhole close to its periphery will be cut off. This small correction has been neglected.

To estimate the effects of space charge within the probe we calculate the radial electric field at the edge of the beam. For the maximum beam densities obtained the field is about 1 v/cm. This is generally much less than the fields resulting from the applied grid voltages and it is concluded that space charge effects are unimportant.

The question of sheath potentials is a complex one. It will be noted that in as much as the analysis above is valid for the relationship between log N and V the value of the electron temperature obtained is independent of sheath potentials, though they may have a large effect on the flux of electrons through the pinhole. Any space charge fields in the region of the pinhole will inhibit the flow of electrons so that the value of n_e obtained from equation 7 must be regarded as a lower limit. The condition that the plasma loses ions and electrons at the same rate in the pinhole aperture region implies that flux of electrons through the pinhole is limited by ion rather than electron mobility. This conclusion is valid independent of the ratio of the pinhole diameter to the sheath thickness.*

i.e. at the pinhole

$$j_e = j_i = \frac{Z_i e n_i \bar{v}_{\parallel i}}{4} \qquad \text{where } Z_i e = \text{ionic charge.}$$

and assuming $T_e = T_i$

$$n_e = 4 \cdot \frac{j_e}{\bar{v}_{\parallel e}} \cdot \left(\frac{m_i}{m_e}\right)^{\frac{1}{2}}$$

where j_e is the measured current density at the phosphor. For a deuterium plasma $\left(\frac{m_i}{m_e}\right)^{\frac{1}{2}} = 60$

Thus

$$n_e = \frac{240\, j_e}{\bar{v}_{\parallel e} \cdot e} \qquad (8)$$

The effect of the probe on the gross characteristics of the plasma are small. The probe surface area is 0.05% of the liner surface area and it projects into the plasma only one twentieth of the liner bore diameter. The local perturbations in the region of the probe are however not easy to estimate. The errors involved depend on the rate of diffusion both across and along the magnetic field and no account is taken of these.

---

* The sheath thickness for zero magnetic field is given by $6.9 (T_e/n_e)^{\frac{1}{2}}$ (Spitzer 1956). For $n_e = 10^{13}$/cc and $T_e = 5 \times 10^6$ °K this is 1.6×10^{-3} cms. The pinhole diameter, d, is 12×10^{-3} cm, i.e. about one order of magnitude greater. At higher densities the electron temperature is less than 5×10^5 °K so under these conditions the sheath is negligibly thin compared with d.

3.4. Results

Electrons are detected at the walls from 400 μ sec after breakdown to the end of the pulse. Since the aperture of the probe is limited it is not possible to cover the whole of this period with the probe in one position. Figure 6 shows a typical probe signal.

Measurements have been made of the electron density calculated from equation (8) using the probe and these have been compared with estimates made by microwave measurements (D.A. Wort private communication). The electron detector gave a mean $n_e = 4.6 \pm 0.8 \times 10^{13}$/cc. The microwave reflection indicated $n_e > 1.5 \times 10^{13}$/cc under the same conditions. The initial discharge pressure was such as to give $n_e = 4 \times 10^{13}$/cc assuming no pinching of the plasma.

The energy of the electrons at the wall is very dependent on discharge conditions. Under low pressure conditions for which energy loss by radiation is unimportant (see § 2) the electron density is high and electron temperatures are between 30 eV and 50 eV, in good agreement with spectroscopic estimates. In figs. 7 and 8 are plotted the experimental results for the relationship, (6) in Section 3.3 The points shown are averages of ten or fifteen discharges. Under all conditions designated Mode 'C' a linear relationship is obtained, permitting an accurate determination of the electron temperature and confirming that the distribution is Maxwellian.

The electron temperatures measured are sensitive to the degree of impurity in the discharge. The addition of 5% argon to deuterium at $\frac{1}{2}$ micron reduces the electron temperature at the wall, as measured by the probe from about 40 eV to 10 eV. Increasing the argon to 15% results in a further drop to 7 eV. From the total radiation measurements it is to be anticipated that the plasma is radiation cooled in this later condition.

In Table III the results obtained for n_e and T_e for various conditions are summarized. The values for n_e are obtained using equation 8.

Increasing the pressure to 5 microns reduces T_e to a value too low for the probe to measure accurately but is in the region of 3 eV. Electrons with such low energies are indistinguishable from photoelectrons which may be emitted from the probe or wall.

TABLE III

Pressure	Condenser KV	Te	n_e
$\frac{1}{2}$	5	32.3 (1)	3.2×10^{13}
$\frac{1}{2}$	5	49 (2)	5.4×10^{13}
1	7	26	2.6×10^{13}
1	10	30	-
2	10	14.5	5.6×10^{13}
$\frac{1}{2}$ + 5% Argon	5	10.3	5.8×10^{13}
$\frac{1}{2}$ + 15% Argon	5	7.2	2.8×10^{13}

(1) Te measured 250 μ sec before peak current

(2) Te " " after " "

The remaining values of Te were determined at peak current.

Observations have also been made in Argon at 1/16 and $\frac{1}{2}$ micron. At the lower pressure the results were similar to those in deuterium at about 1-2 micron with the machine conditioned, thus the electron temperature was 17 eV and n_e about 10^{14}/cc. At $\frac{1}{2}$ micron the mean electron energy at the wall was less than 5 eV, a result comparable with discharges in deuterium at about 5 micron. In argon it will be noted (see §2) that radiation losses are small at 1/16 micron but that the plasma is radiation cooled at $\frac{1}{2}$ micron.

Fluctuations

The output from the probe often shows regular fluctuations in the 10-80 kc/s range. These may be due to fluctuations in electron density outside the probe but the possibility that they originate within the probe cannot be ignored. At the residual pressure of the probe, it is known that electron beams are noisy (Cutler 1956). It has not proved practical to reduce the residual pressure low enough to resolve this ambiguity. However, fluctuations in this frequency range are observed with magnetic search coils, and with other devices.

3.5 Estimation of the energy lost to the walls by thermal particles

The finite separation of the axial field coils and fluctuations in the discharge both produce a radial component of magnetic field at the liner. Plasma may therefore diffuse along the lines of force to the wall at the regions of intersection between the wall and the magnetic field. The fraction of the total liner surface, defined as $\bar{\alpha}$, connected by the field to the plasma in this way is given by $\frac{B_r}{B_{\theta z}}$ where B_r is the mean radial component of magnetic field and $B_{\theta z}$ is the tangential component.

Taking the particle flux along the field lines to be given by $\frac{1}{4} n_a \bar{V}_a$ (where n_a is the density of particle specie a and $\bar{V}_a$ is its mean thermal speed) we have calculated the $\bar{\alpha}$ required to give a particular energy transfer to the liner. We have made this calculation for two assumptions about the wall potential.

1) There is a sheath potential of order 4 kTe

2) Arc spots prevent sheath formation and the potential difference between the plasma and the liner is given by the arc voltage, taken to be 20 volts. The energy dissipated in the plasma by the arc current electrons has been taken into account.+

The results of these calculations show that for a plasma density of 2×10^{13}/cc with a mean energy of 40 eV we require $\bar{\alpha} = 0.06$ in case 1 to account for the energy loss. For the second case the $\bar{\alpha}$ required is 0.05. The inhomogeneity produced by the B_z field coils gives an $\bar{\alpha}$ of approximately 0.05. This calculation gives a maximum estimate of $\bar{\alpha}$ since diffusion across the lines of force has been ignored. If the electrons detected at higher pressures (i.e. 5 microns) in deuterium discharges are part of the plasma rather photo electrons then for these conditions the value of $\bar{\alpha}$ required to account for the energy loss is about unity.

+ The form of energy loss by particles calculated from the two assumptions concerning the wall/plasma boundary potential is very different in the two cases. In case 1 the energy transported to the walls by ions is about six times that carried by the electrons, since the ions are accelerated through the boundary sheath whilst the electrons are retarded. In case 2 the electrons are lost at a greater rate than the ions due to their greater thermal velocity. Plasma neutrality is maintained by the arc current electrons. Under these conditions the energy flux to the walls carried by the electrons is about seven times that of the ions.

Thus at low pressures the required $\bar{\alpha}$ is only little in excess of that produced by the B_z field coils whilst at high pressures an impossibly large value of $\bar{\alpha}$ is needed. The work of Burton and Wilson (1961) has, in fact, shown that ion containment times are increased at higher particle density. In the absence of large plasma-wall arc currents this increase holds for the electrons also. The longer containment times at higher pressures together with the low electron energies observed indicates that loss of plasma at these pressures contributes less than 10% to the energy loss.

From the preceding discussion it may be concluded that the energy loss resulting from the limited containment of the plasma is dominant at low pressures but becomes unimportant as the operating pressure is raised to five microns. This behaviour may be contrasted to the radiation loss for which the inverse variation is observed.

3.6 Plasma diffusion

In order to maintain the observed high density at the wall a high rate of diffusion of plasma from the central region is necessary. Such a diffusion has been deduced from spectroscopic observations (Burton and Wilson 1961).

It has been suggested (Spitzer 1960) that the rapid diffusion of plasma observed in thermonuclear research devices may arise through non thermal fluctuating electric fields in the plasma. These electric fields produce the well known $\underline{E} \times \underline{B}$ drift and diffusion of the plasma results.

We have made a preliminary investigation with simple electrostatic probes of the Zeta plasma. The experimental results of this investigation are summarized below.

1) Electric fields exist, in the plasma, of up to approximately 50 v/cm. They are correlated over distances of the order 10 cms and are principally transverse to the magnetic field lines. The frequencies are in the range 20 - 80 Kc/s the lower frequencies appearing at the higher pressures.

2) The fields fall rapidly in amplitude as the pressure increases. The amplitude at 5 micron being about one tenth that at $\frac{1}{2}$ micron.

3) The fields have been observed in H_2, A, D_2 and He. In Argon the pressure required to produce similar amplitudes to those present in D_2 at $\frac{1}{2}$ micron is 1/16 micron.

Simple calculations show that the fields are of the right order to account for the rapid diffusion and they are greatest in amplitude when the observed radiation losses are small.

3.7 Thermal energy containment time

From the observed electron temperatures (and equating T_i to T_e) we may estimate the thermal energy stored in the plasma. Measurements of the total energy supplied to the plasma and the amount lost by radiation then enables us to calculate approximate energy containment times for the particles of the plasma.

Thus:

Thermal energy + ionisation energy in plasma

$= n.V.[k(T_i + T_e) + \phi]$ $\quad V$ = volume of plasma

ϕ = ionisation energy

Energy supplied to particles throughout pulse

= W - R where W = total energy input to plasma

R = Radiated energy + fast electron loss

Then if t = pulse length and $T_e = T_i$

approximate containment time Δ t is given by

$$\Delta t/t = n.V.\ (2kT_e + \phi)/W - R.$$

The results obtained from this formula, using the values of Te from Table III are shown in Table IV.

Table IV

Pressure	KV	W joules	R joules	$\Delta t/t$	pulse length t_{obs} msec	Δt μsec
$\frac{1}{2}$	5	5.2×10^4	2.3×10^4	0.138	2.8	386
1	7	8.2×10^4	2.9×10^4	0.100	3.3	330
1	10	17.3×10^4	4.3×10^4	0.047	3.0	140
2	10	17.2×10^4	8.7×10^4	0.066	4.2	276

The Δ t values calculated above are essentially the times required for an electron or ion to deposit its thermal energy at the liner. They are necessarily crude estimates since T_i and n_e are not known accurately.

For the two cases at 10 kV, ion containment times have been measured by Burton and Wilson (1961) and these are about 30% longer than the corresponding values of Δt. If this difference between the thermal energy containment time and the ion containment time is significant then we may conclude that either $T_i > T_e$ or that on average each particle carries more than its associated thermal energy to the wall. In view of the possibility of sheath formation at the wall the second alternative cannot be ruled out.

3.8 Detection of non thermal electrons

For discharges in Mode D at low pressure, i.e. less than 1 micron, a divergence from the Maxwellian relationship is clearly indicated (see fig. 8a) Fig. 9 illustrates the difference between the two modes. In Mode D runaway electrons accelerated by the applied electric field can enter the probe, in Mode C they cannot. One concludes that there is a non thermal tail to the electron distribution which consists of electrons streaming in the direction of the convection current. Fig. 8b shows that at 2 microns this tail is absent. Stray pick up on the probe signal determines how much of the distribution can be plotted. The signal/noise ratio is unity at about 5 T_e volts on g_2. By increasing the photomultiplier voltage the sensitivity of the probe can be increased x 200 and in this way it has been shown that in Mode D there is a detectable number of electrons present at $\frac{1}{2}$ micron, with energies greater than 1 keV, from peak current onwards. No such flux of high energy electrons is detectable in Mode C operation.

The apparent anisotropy of the electron energy distribution at low pressures shown in fig. 8a may be connected with the non-thermal behaviour of the plasma. Observations of impurity ion energies by Doppler broadening (Butt et al 1958) and electrostatic probe measurements (see 3.6) also indicate the presence of non-thermal processes under these conditions. These experiments too, show that non-thermal processes are suppressed by increasing the operating pressure.

The population of the non-Maxwellian tail of the distribution increases over the last millisecond of the current pulse and it is logical to assume that the burst of X-rays observed at the discontinuity in the plasma current is a catastrophic manifestation of this effect.

§ 4 Energy Loss by Non-Thermal Electrons above 2 keV

Colgate et al (1958) have suggested that energy loss due to electrons in this energy range can be an important process. In this section we shall show that in Zeta this source of energy loss is important only at the time of the terminal current discontinuity, which occurs only at low pressures (< 2 microns).

We have investigated energy loss by fast electrons by examining the X-rays they produce when they strike the stainless steel liner of Zeta. Measurements have been made to determine the conditions and time in the current pulse for which fast electron loss is important, the magnitude of the loss and the energy of the electrons.

4.1 Experimental Methods

Scintillation Counter

Time resolved oscillograms of the X-ray production can be obtained by means of an X-ray scintillator. For energy loss measurements the scintillator is deliberately made to have a low sensitivity and depends for its operation on the "pile up" of many X-ray photons within the collection time of the phosphor ($10^{-8} \rightarrow 10^{-6}$ secs dependent on the phosphor). The device is sensitive to X-rays produced by electrons harder than 2 keV at intensities of the order of 10^6 times smaller than those observed in Zeta. It is shown in fig. 10. The scintillator can observe various regions on the inside wall and on the bottom of the torus.

Film Exposures

An apparatus (fig.11) has been constructed to expose casettes of X-ray film 6 mm further from the discharge than the level of the liner. Each casette is fitted with a collimating disc of stainless steel which defines a viewing angle of 45°. The casette is positioned so that all X-rays within this angle come from the opposite (inside) wall of the torus and not from nearby objects on the outside wall. To reduce fogging caused by X-rays produced by electron bombardment of the casette itself, it has a front foil of 5×10^{-3} inch beryllium. It has been verified in the laboratory, that electron bombardment levels similar to those incident on the Zeta liner (see §4.2) produce no appreciable fogging. The combined transmission of the beryllium and of the 2×10^{-4} inch aluminium light seal is 1% at 2 keV.

Various thicknesses of absorber placed in the casettes, each casette normally carried four absorbers, provided data yielding an X-ray absorption curve. This curve can be compared with absorption curves obtained using a simple X-ray set having a target of the same material as the Zeta liner. By selecting a suitable electron energy or combination of energies in the X-ray set it is possible to reproduce the Zeta curve and thus to deduce approximately the Zeta electron energy spectrum.

The X-ray set has also been used to calibrate the film† used on Zeta and, in this way, by using a calibration curve for the correct electron energy, the intensity of the fast electron wall bombardment in Zeta was estimated.

4.2 Experimental Results

X-rays emitted from Zeta have all energies from 1 keV or so up to 1 MeV or more (Harding et al 1958), however only those having energies in the few kilovolt range are intense enough for the electrons which generate them to carry an appreciable fraction of the discharge energy to the walls. Pinhole X-ray photographs in this energy range clearly show the wall structure of the torus interior, this implies that the X-rays are produced by electrons striking the stainless steel liner. Projections into the torus, such as Rogowski coils emit more copiously than the surrounding wall, and so to a lesser extent do wall irregularities such as joins of liner sections.*

Time of Emission

X-rays are emitted in two groups, one of low intensity at the beginning of the pulse associated with the breakdown of the gas and one of much greater intensity at the end of the pulse associated with the terminal current discontinuity. The scintillator observations indicate that the first burst makes no appreciable contribution to the total X-ray intensity. The second burst of X-rays always reaches its maximum intensity at the current discontinuity, much smaller intensities are present immediately before and after the discontinuity. An example is shown in fig.12. Typically the most intense X-ray emission is complete in 1-2 usecs.

---

† We are grateful to E.S. Hotston for generously making available his independent X-ray film calibrations and his observations on the efficiency of X-ray production.

* These observations are supported by a more extensive series of pinhole photographs due to H.C. Cole and E.S. Hotston.

These observations indicate that during the bulk of the current pulse the amount of energy carried to the walls by electrons with energy greater than 2 keV is negligible. However at the end of the current pulse fast electron loss is important. The maximum possible energy for fast electron production is the change in stored magnetic energy at the current discontinuity, plus, possibly the inductive energy stored in the external circuit at this time, although most of this energy seems to be dissipated after the most intense X-ray emission is over. The change in magnetic energy at the current discontinuity is of the order of 20% of the total input energy and the inductive energy released from the external circuit at this time is about 10% of the total input energy.

Intensity Measurements

Absolute intensity measurements made by film, and relative intensity measurements made using scintillators, show a wide shot to shot variation. A histogram obtained from 109 film exposures (three discharges/exposure) is shown in fig.13. Similar histograms have been obtained from scintillator measurements. The horizontal scale in the figure is calculated on the assumption of uniform wall bombardment. Since, on this assumption the largest possible value of the abscissa is 20% of the energy input, it is likely that the observed variation is due to the electrons being deposited on local areas of wall, the particular region varying from shot to shot.

The mean level derived from the histogram is about 60% of the energy input, this is about three times the energy available at the current discontinuity. This suggests that the inside wall of the torus receives more fast electron bombardment than other parts. Scintillators looking at different areas (100 cm diameter circles) of the inside wall show the same mean level of bombardment (averaged over many discharges). A scintillator looking vertically at a 100 cm diameter circle on the bottom of the torus indicates bombardment which can be similar to or much less than that observed on the inside wall, whether a large or a small bombardment is observed depends upon the discharge parameters and in particular conditions, on the direction of the axial stabilizing field.

These results indicate that the major part of the total energy present in the tube at the current discontinuity is lost as fast electrons.

Variation with Pressure

As the pressure increases the X-ray intensity dimishes until at pressures above 2 microns X-rays are not detected at the end of the current pulse and fast electrons do not therefore contribute to the energy loss. Under these conditions there is no current discontinuity.

Variation with Bz

As B_z is increased a critical B_z is reached where both the current discontinuity and the X-rays disappear, this critical value is somewhat less than the B_z necessary to prevent pinching and with 10 kV on the 3 MJ bank is around 1000 Gauss.

Absorption Measurements

These results are presented in Fig.14.

It will be seen that it is easy to pick a mean energy for the electrons in Zeta, although it is not possible, without further work, to exclude the possibility of small contributions from other energy groups. To illustrate this a combined curve from the X-ray set (90% 8 kV., 10% 10 kV.) is shown: it is a good fit to the Zeta curve at 10 kV, 500 amps B_z, $\frac{1}{2}$ u D_2 which would also be fitted by a single energy between 8 and 8.5 keV.

The energy obtained for a number of conditions is shown in Table V..

TABLE V.†

Zeta Conditions			Electron Energy keV	Change in Magnetic Energy per Electron at Current discontinuity keV
Condenser Bank Voltage kV	B_z field Gauss	Pressure micron		
5	225	0.5	7	2
10	375	0.5	8.4	4
10	375	1.0	8.4	-
10	525	0.5	9.3	6
10	750	0.5	10	6

† These results are confirmed by the work of E.S. Hotston using a novel technique based on the critical reflection of X-rays (Hotston 1961).

4.3 Electron runaway at the current discontinuity

W. Burton and R. Wilson (1961) show that the current discontinuity occurs when "pumpout" has reduced the particle density to $n_i = n_e = 9 \times 10^{12}$/cc (pressure ~ 0.13 micron) and this is confirmed by microwave measurements (D.H.J. Wort 1960).

The electron temperature will probably not differ greatly from that at peak current i.e. Te ~ 5×10^5 °K (Butt et al 1958). It is possible to estimate that the resistive electric field immediately before the current discontinuity is around 0.5 V/cm.

X = electric field volts/cm

Thus $\frac{X\ Te}{n_i} = \frac{0.5 \times 5 \times 10^5}{9 \times 10^{12}} \sim 3 \times 10^{-8}$ Te = electron temperature

Ni = ion density/cc

For more than 0.1% of the electron flux to become decoupled from the ions and "runaway" we require $\frac{X\ Te}{n_i} > 10^{-8}$ †

Thus we see that immediately before the current discontinuity runaway has become an important process, as the runaways escape from the discharge they will cause a further reduction in density and hence more runaway until the process becomes catastrophic.

4.4 Acceleration times and permissible runaway currents

Experimentally the duration of the current discontinuity is of the order of 2→5 μsec. Most of the X-ray emission takes place within 2 μsec. It is interesting to compare this time with the acceleration times of the electrons.

The resistive electric field present during the discontinuity is not likely to be at all similar to that existing earlier, and it is difficult to estimate its magnitude. The voltage around the discharge V_L at the discontinuity can be measured, it is positive, and at ½ micron pressure is typically of the order of 5 kV per turn with the condenser bank initially charged to 10 kV. We have:

$$V_L = V_R + L\, dI/dt + I\, dL/dt \qquad (9)$$

---

† The formula given by Gibson (1957) has been modified to include electron - electron collisions and to use the Spitzer expression for the mean free path.

V_R = resistive voltage drop per turn

L = discharge inductance

I = current

The second term in equation (9) is negative and typically of the order of -10^5 volts/turn (taking I to fall by 100 kA in 3 μsecs and L to be 3 μH). Little is known experimentally about the third term in equation (9) and it could in principle be either positive or negative, however over the whole discontinuity L must fall from an initial value in the region of 3 μH (calculated from the magnetic field configurations (Lees & Rusbridge 1959) to a low value. If we use this behaviour to estimate a mean value for $I\, dL/dt$ we find $I\, dL/dt \sim -10^5$ volts/turn. Thus we see the resistive field available to accelerate electrons during the current discontinuity is of the order of 10^5 volts/cm. The corresponding acceleration time to 8 keV is 3×10^{-8} secs.

Short acceleration times of this order are in fact necessary if very large currents are not to flow at the discontinuity. Consider, for example that each electron is accelerated in a time τ to an energy of 8 keV and then escapes from the discharge. If the electrons travel in the z direction we require $\tau < 10^{-8}$ secs in order that the I_z produced be < 250 kA. If the electrons travel in the θ direction we require $\tau < 6 \times 10^{-9}$ secs in order that the B_z produced be < 1000 Gauss ($I_\theta < 750$ kA). Thus we require the electrons to be lost progressively and at any one time less than 1% of the electrons will be "running away".

4.5 Energy per Electron at the current discontinuity

If all the electrons initially present at the current discontinuity eventually run away and produce fast electrons, one would expect that the change in magnetic energy at the discontinuity divided by the total number of electrons present (9×10^{12}/cc see section 4.3 above) would be equal to the observed electron energy. The figures obtained from this calculation are compared with the experimental results in Table V

It will be noticed that the experimental energies at Vc = 10 kV are too big by about a factor 2. The errors in the calculation might conceivably be as big as this, thus the magnetic energies have been estimated from probe measurements (Lees & Rusbridge 1959). on the current rise by assuming that, for the same ratio of current to initial B_z, the same configuration will exist at the

discontinuity as exists on the current rise. However if the effect is a real one then it implies that only about half the electrons present at the discontinuity reach the wall with large energies (> 2 keV).

§ 5 Discussion

The scaling laws for the stabilised pinch have been discussed by Bickerton and London (1958) and it might be hoped that the application of these laws should produce some universal conclusions, when applied to the pinch machines studied. The scaling laws have, of course, been derived from classical magneto-hydrodynamics whereas we have conclusive evidence that the plasmas in these machines do not behave in a classical way (for example: neutrons, ion energies, anomalous resistivity, diffusion). We can, therefore, draw only the broadest conclusions about the behaviour of pinch devices.

In the following table are tabulated the more important parameters of four pinch machines and the scaling laws relevant to energy loss that have been applied to them are given below.

1) Radiation loss rate $\propto N^2R^{-2} f(Te)$ where N = line density
R = bore radius
f(Te) = function of electron temp.

2) Particle loss rate due to thermal instability (Butt et al 1958) $\propto NR^{-2} . Te^{-\frac{1}{2}}$

3) Condition for runaway electrons $\propto$

$$\frac{v_D}{v_{TH}} \propto \frac{I}{NTe^{\frac{1}{2}}}$$

v_D = electron drift velocity
v_{TH} = electron thermal velocity
I = gas current

TABLE VI

	Zeta	Sceptre	PS-4	Gamma
pressure (microns)	0.5 - 5.0	0.5 - 5.0	20 - 200	5 - 50
radius (cms)	50	15	7	5
gas current K.A.	200	200	200	200
N^2/R^2 *	1	0.09	30	1
N/R^2 *	1	1	40	10
I/N * +	1	11* 2.7+	1.3* 0.3+	10* 2.5+
time to peak current (μsec)	1000	250	10	10
Energy/particle/μsec*	1	1	40	100

* Normalised to Zeta value at $\frac{1}{2}$ micron
\+ " " " " " $\frac{1}{2}$ micron

The runaway condition has been normalised to $\frac{1}{8}$ micron since this is the equivalent pressure at the end of the current pulse when catastrophic runaway occurs in Zeta.

From the ratios given in the table we may, in a empirical way, predict the dominant loss processes for the published operating conditions in Sceptre, P-S4 and Gamma. The conclusions are as follows.

	Sceptre	P-S4	Gamma
Radiation	Not important	Important at high pressures	Not important
Particle loss	Important especially at low pressure	Important at low pressures	Not important
Runaways	Important at low pressures	Not important	Important at low pressure

The runaway condition was violated to a greater extent in Gamma and Sceptre than in the other two devices. A large runaway electron flux has been observed in Gamma but not in Sceptre. In P-S4 both radiation and particle loss rates are greater than in Zeta and this is almost exactly compensated for by the greater rate of energy input into the discharge. Thus one expects P-S4 to have similar particle energies to those observed in Zeta. Runaway electrons are unlikely to be produced in this machine.

§ 6 Conclusion

There are two regimes of energy loss from Zeta discharges in deuterium; one is operative at high pressures e.g. 5 microns) and one at low pressures (e.g. 0.5 microns); this is illustrated in fig.15 where the observed loss processes are summarized and presented as a function of time during the current pulse.

At high pressures radiation is the dominant loss process and under certain conditions, at pressures above 5 microns, accounts for the total energy input. This radiation is in the vacuum ultra violet in the region below 1500 Å. The variation of impurity line radiation intensity with pressure (Burton 1960) is similar to that for the observed total radiation, suggesting that impurities are an important source of radiation. Theoretical considerations show that the observed impurity content (Griffin 1961) of 10^{11} atoms/cc can account for the observed radiation intensity. Electrons detected at the wall at these high pressures cannot be distinguished from photo-electrons, but are in any case of too small an energy and density to cause an appreciable loss.

At low pressures, a large density ($> 10^{13}$/cc) of thermal electrons, with mean energies between 30 and 50 eV, is detected at the walls. In order to be present in such high densities these electrons must form part of a plasma, which, in this region, where the magnetic field lines are connected to the torus wall, transfers energy to the wall fast enough to account for the energy input. This conclusion is in agreement with the work of Burton and Wilson (1961) who have determined the plasma loss rate from spectroscopic observations. In order to maintain the observed high density of plasma at the wall there must be a rapid diffusion of plasma from the centre of the discharge. Observations are described which show that fluctuating electric fields, large enough to produce this diffusion are present in the plasma.

The termination of the current pulse at low pressures is catastrophic, the current falling from some 200 KA to a low value in 2 μsecs. This discontinuity is accompanied by an intense burst of X-rays emitted from the torus liner. The fast electrons which generate these X-rays have an energy of about 8 keV and carry to the walls the magnetic energy which is present immediately before the discontinuity. The work of Burton and Wilson (1961) has shown that the particle density at the discontinuity is 9×10^{12}/cc.,

and under these circumstances electron runaway becomes important (Gibson 1957). We have shown that a consistant explanation of the current discontinuity is possible in terms of catastrophic runaway.

Energy loss from Argon discharges is essentially similar to that in deuterium but with a different pressure scale. Radiation is the dominant loss at pressures greater than 0.5 microns, the radiation falls off at lower pressures and at 1/16 micron the electron detector indicates a high density of electrons at the wall with an electron temperature of 17 eV, the current discontinuity and associated X-rays appear.

Acknowledgements

We are grateful to Mr. R.S. Pease for suggesting the problem and for much helpful discussion. Dr. G. Barsanti[*] contributed to the experiments on X-ray emission. Dr. B. W. Ridley suggested the scintillation technique used to detect low energy electrons. The electrical characteristics, including the energy input to the discharge, were measured by Mr. E. P. Butt and his colleagues. The special electronic equipment used was designed by Mr. R. Jenkin and the engineering design of the apparatus used was by Mr. D. Booker and Mr. J. Bradley. Finally it is a pleasure to acknowledge the assistance of Mr. M. J. Forrest, Mr. M. Hill, Mr. B. M. White and that of the Zeta Operations Group.

[*] C.A.M.E. Laboratory, Livorno, Italy.

REFERENCES

Allen, C.W. 1960. Proc. Liege Conf. Les Spectres des Astres dans Ultra Violet Lointain.

Allibone, T.E., Chick, D.R., Thompson, G.P., Ware, A.A., 1958. Proc. of the Geneva Conf. 32 169.

Bernstein, W., Kranz, A.Z., 1959. Phys. of Fluids 2, 57.

Bickerton, R.J., London, H., 1958. Proc. Phys. Soc. 72, 116.

Burton, W.M., 1960 Private Communication.

Burton, W.M., Wilson, R. 1961 to be published Proc. Phys. Soc.

Butt, E.P., Carruthers, R., Mitchell, J.T.D., Pease, R.S., Thonemann, P.C., Bird, M.A., Blears, J., Hartill, E.R., 1958. Proc. of the Geneva Conf. 32, 42.

Collgate, S.A., Ferguson, J.P., Furth, H.P., Proc. of the Geneva Conf. 32 129.

Corner, J.P., Hagerman, D.C., Honsaker, J.L., Karr, H.J., Mize, J.P., Osher, J.E., Phillips, J.A., Stovall, Jr. E.J., 1958 Proc. Geneva Conf. 32 297.

Cutler, C.C., 1956. Proc. Inst. Radio. Eng. N.Y. 44, 61.

Dellis, A.N., 1961 Private Communication.

Dolgor-Saveliev, G.G., Ivanov, D.P., Mukhovatov, V.S., Razumova, K.A., Strelkov, V.S., Shepelyev, M.N., Yavlinsky, N.A., Proc. Geneva Conf. 32 82.

Gibson, A. 1957. Proc. of the 3rd Int. Conf. on Ionization in Gases Venice.

Gibson, A., Mason, D.W., Barsanti, G., Bull. Am. Phys. Soc. Montreal Conference C-4 1960.

Griffin, W. 1961 private communication

Harding, G.N., Dellis, A.N., Gibson, A., Jones, B., Lees D.J., McWhirter. R.W.P., Ramsden, S.A., Ward, S., 1958 Proc of the Geneva Conf. 32 365.

Harding, G.N., Kimmitt, M.F., Ludlow, J.H., Porteous, P., Prior, A.C., Roberts, V., Proc. Phys. Soc. 77, (1069) 1961.

Hotston, E.S. 1961 U.K.A.E.A. report in course of publication.

Karr, H.J., Knapp, E.A. Osher, J.E. 1961, Phys. of Fluids 4, 424.

Kirillov, V.D., 1960, Z. Tech. Fiziki 5 320.

Knorr, G., 1958 Zeits f.Natur f. 13A 941.

Lees, D.J., Rusbridge, M.C., 1959 Proc. of 4th Int. Conf. on Ionization in Gases Uppsala 1959.

Lees, D.J., Rusbridge, M.C., 1961 to be published at the Salzburg Conference.

Mitchell, J.T.D., Whittle, H.R., Jackson, E.M., Clarke, P.B., 1959 Proc. Inst. Elect. Eng. A 106 (2) 74.

McWhirter, R.W.P. 1960 Private communication.

Spitzer, L. 1956 "Physics of Fully Ionized Gases" Interscience N.Y.

Spitzer, L., 1960 Phys. of Fluids 3, 659.

Watambe, K., Inn, E.C.Y., 1953 J.O.S.A. 43 32.

Wolley, R.v.d.,R., Stibbs, D.W.N.; 1953 "The Outer Layers of a Star" Chap. IV Oxford.

Wort, D.H.J., 1960 private communication.

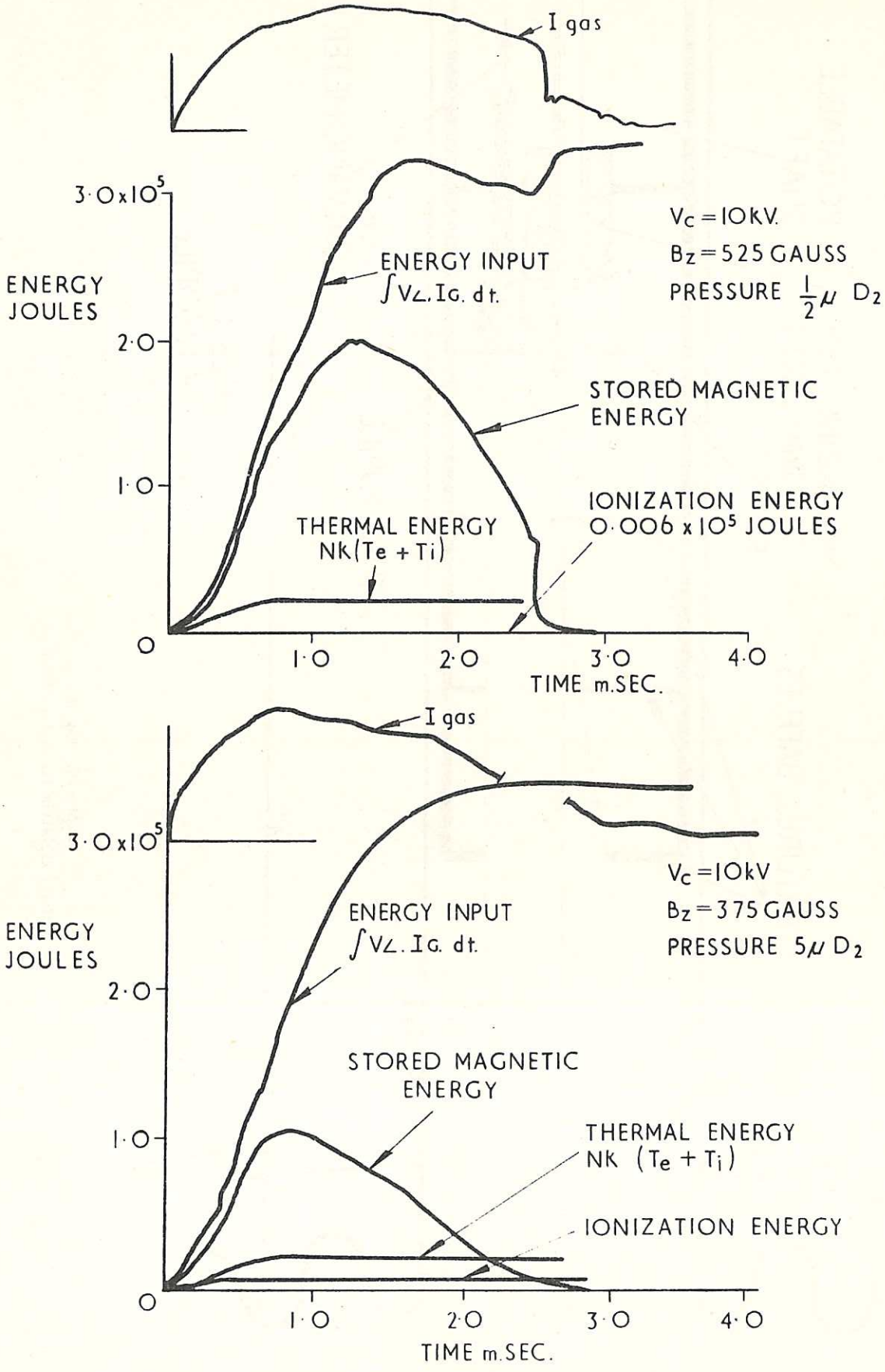

CLM - P2 Fig. 1

Energy input to the discharge as a function of time, together with the estimated magnetic, ionization and thermal energies

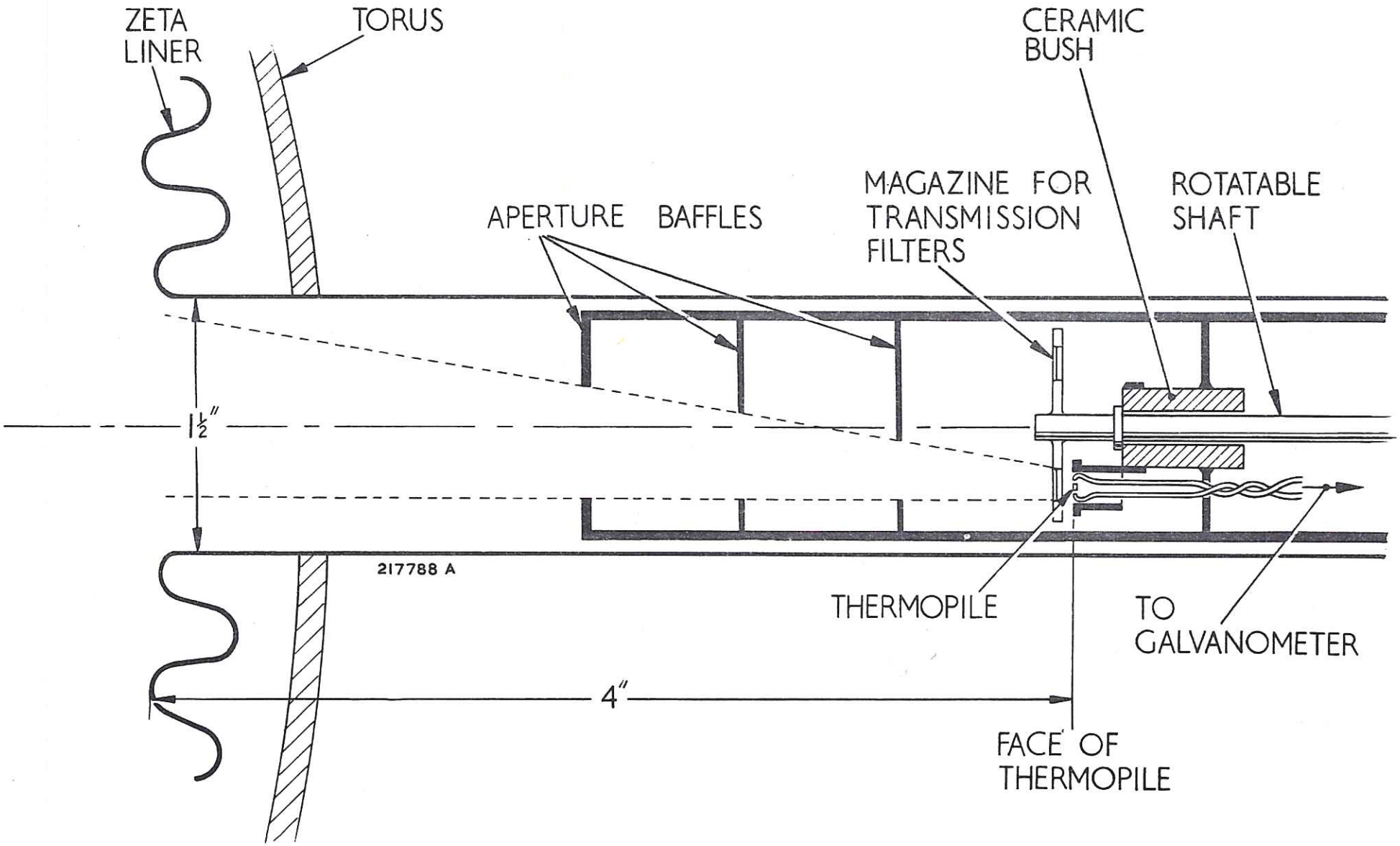

CLM - P2 Fig. 2

Total Radiation Thermopile apparatus

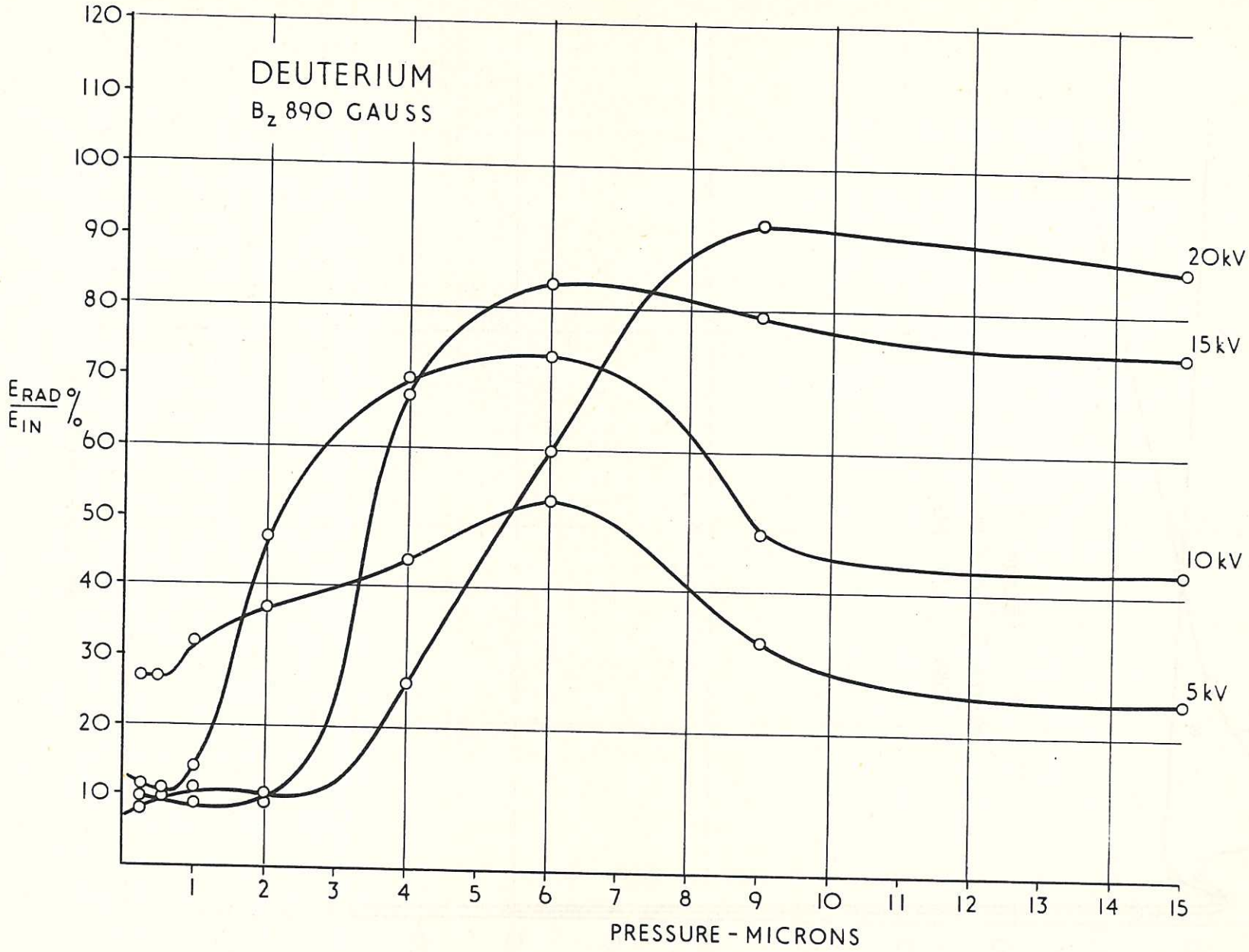

CLM - P2 Fig. 3

Energy radiated as a function of pressure and capacitor bank voltage for discharge in deuterium

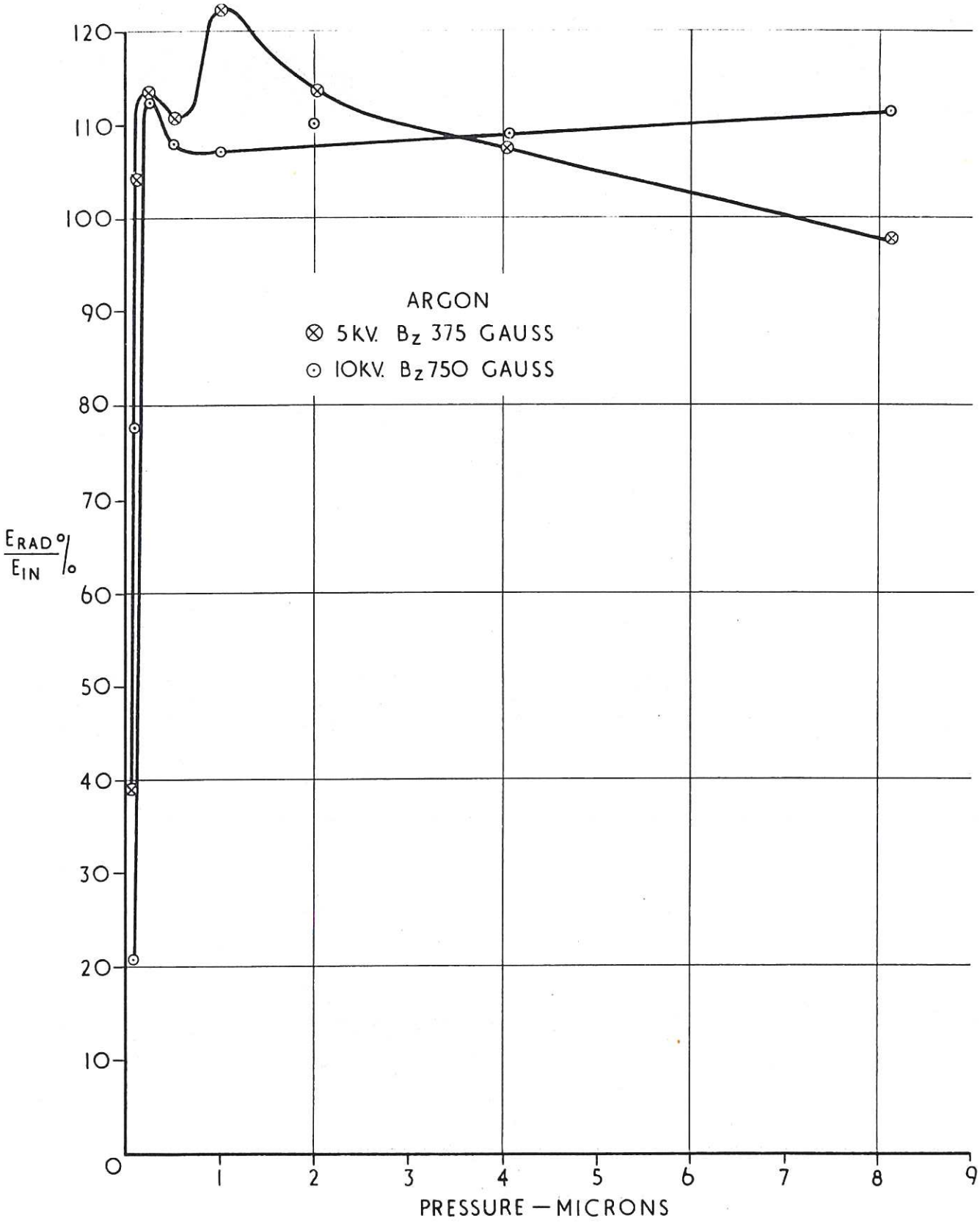

CLM - F2 Fig. 4

Energy radiated as a function of pressure and capacitor bank voltage for discharge in argon

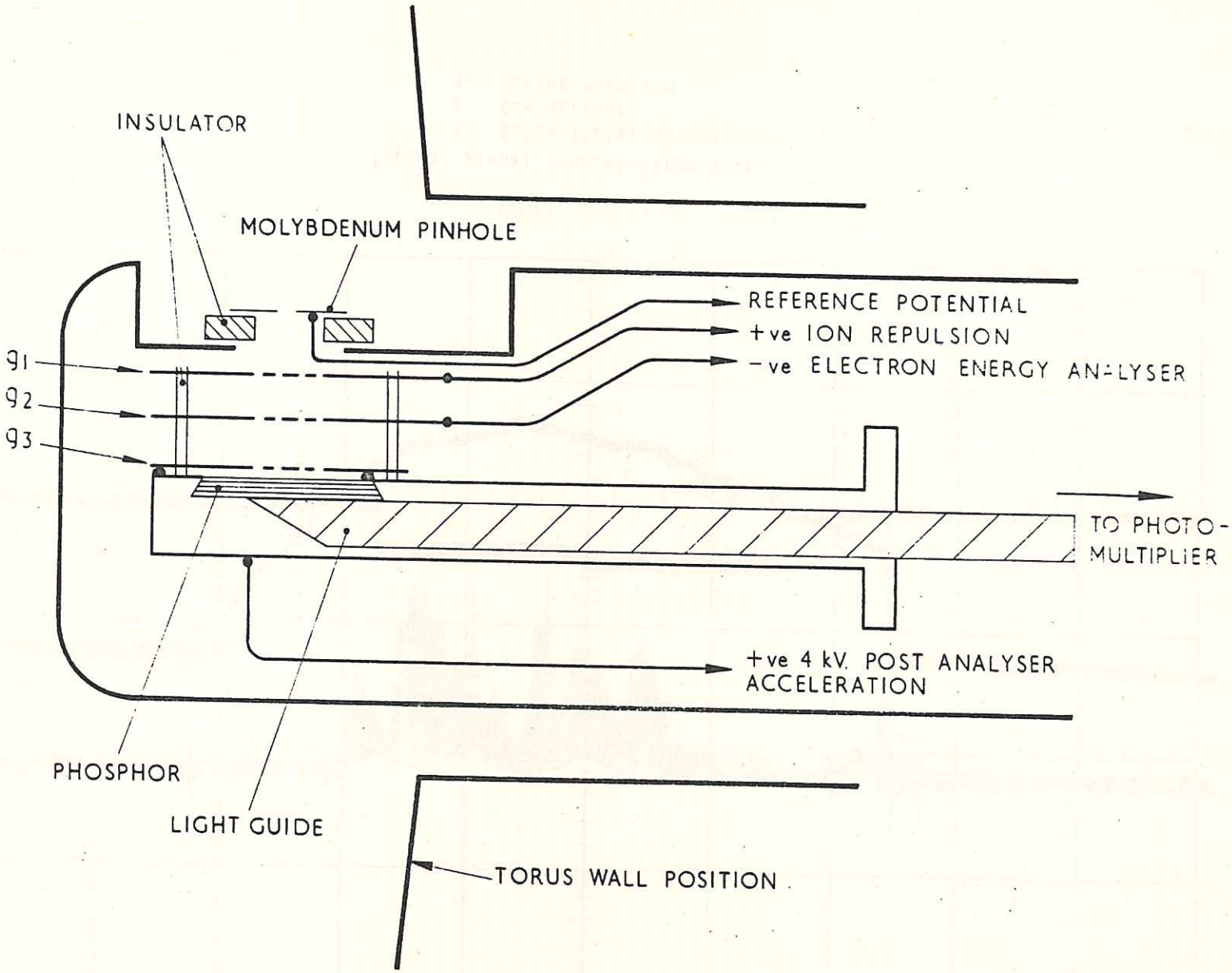

CLM - P2 Fig. 5
Electron detector probe

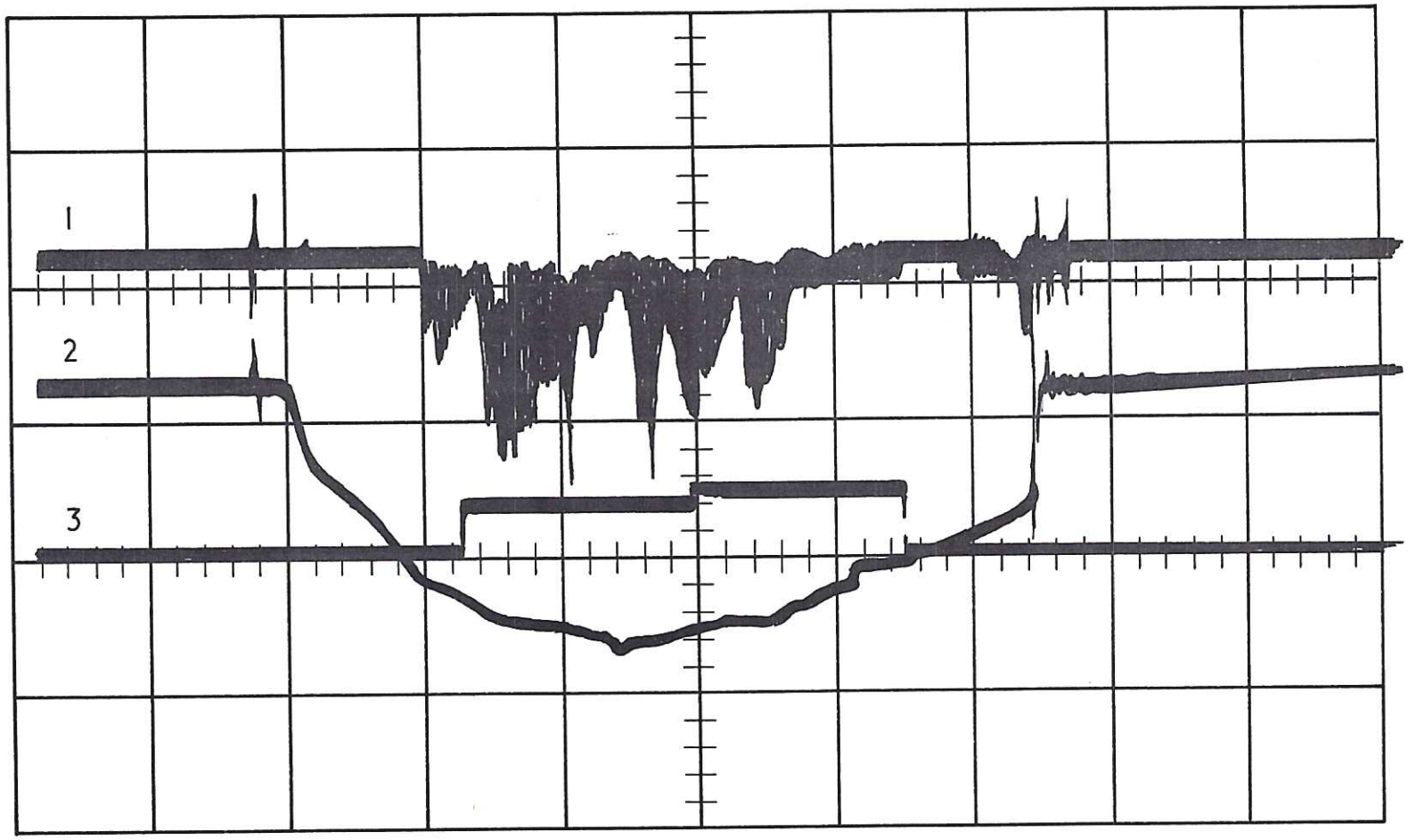

CLM - P2 Fig. 6

Typical signal from electron detector

1. Scintillator output
2. Gas current
3. Gating waveform

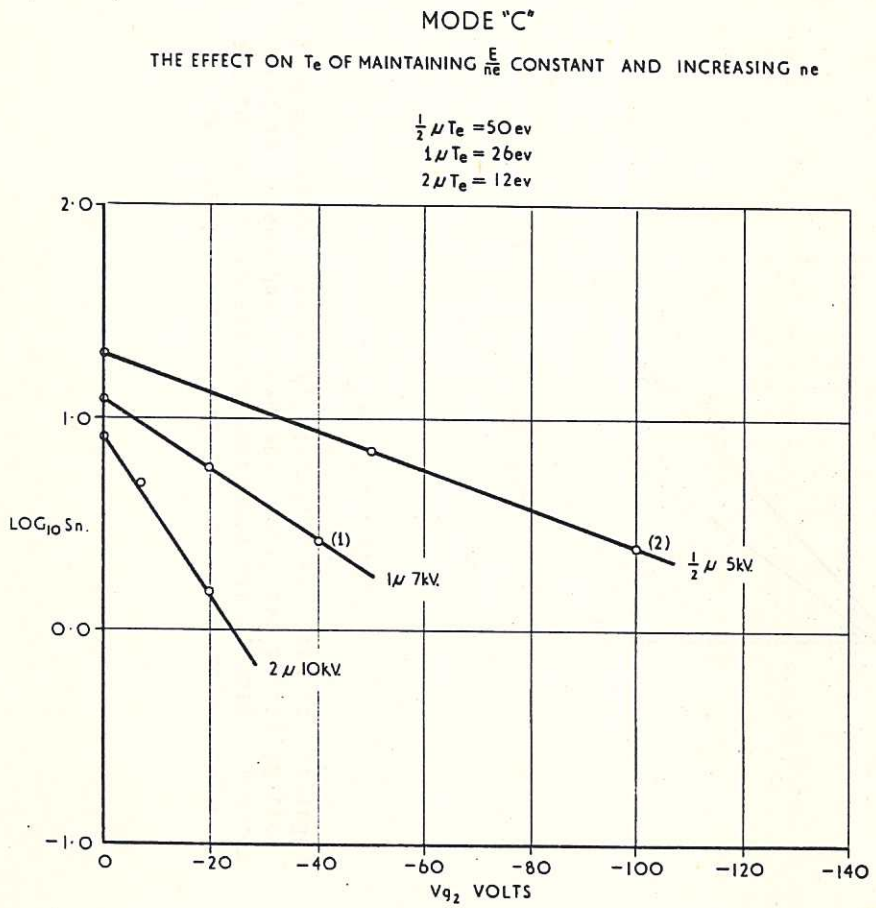

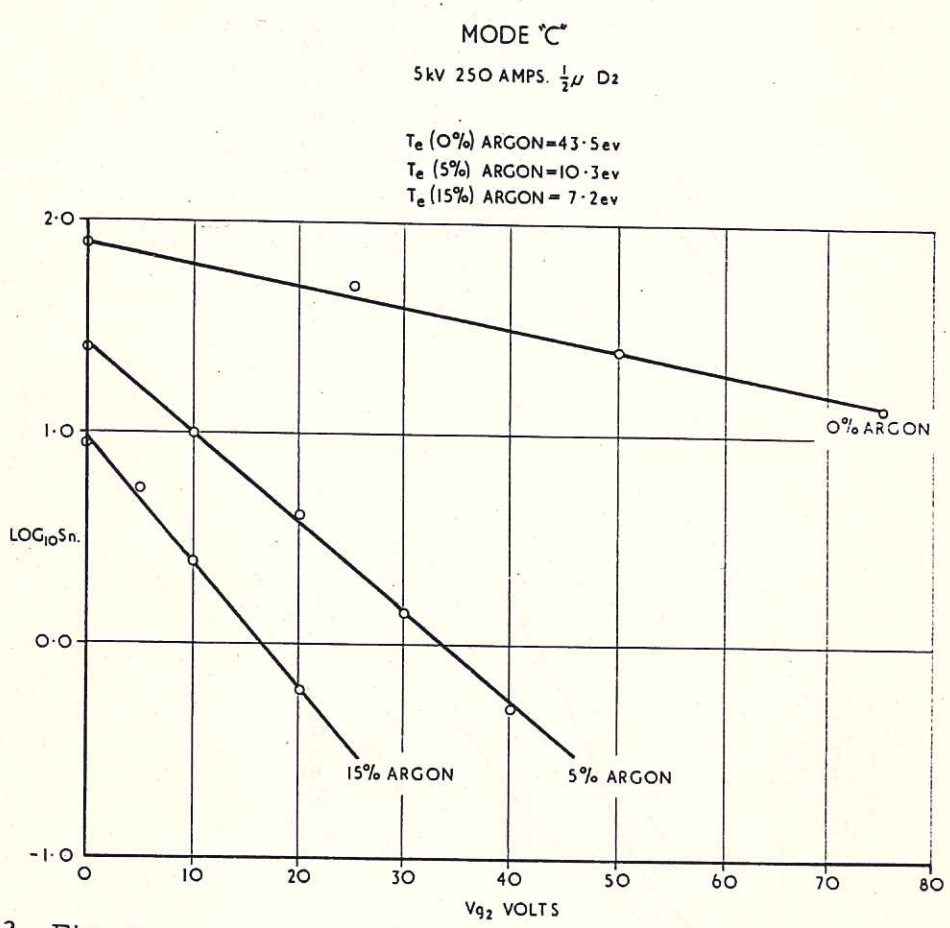

CLM - P2 Fig. 7

Fig. 7(a)

Logarithm of electron detector signal vers analysing grid voltage for discharges in deuterium (a) and deuterium with added argon (b)

Fig. 7(b)

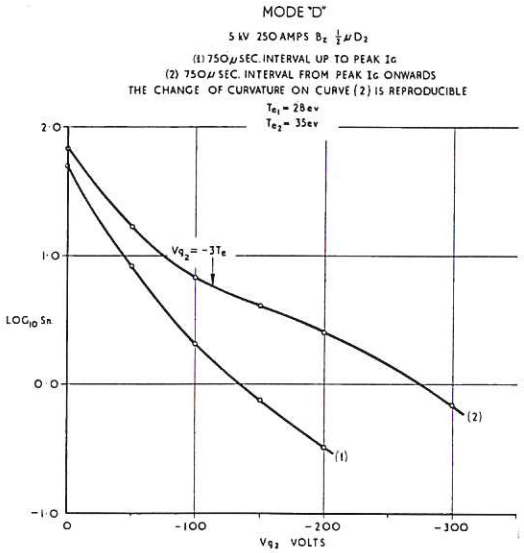

Fig. 8a

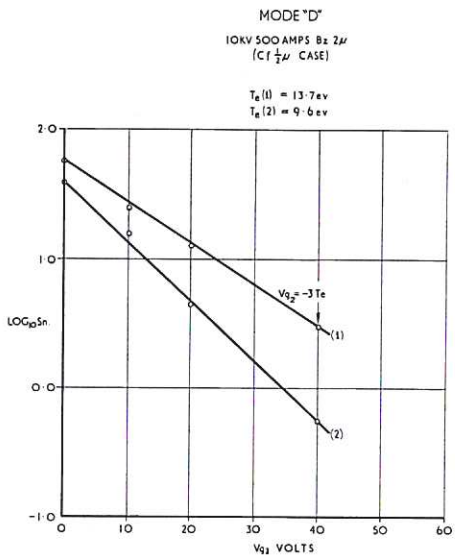

Fig. 8b

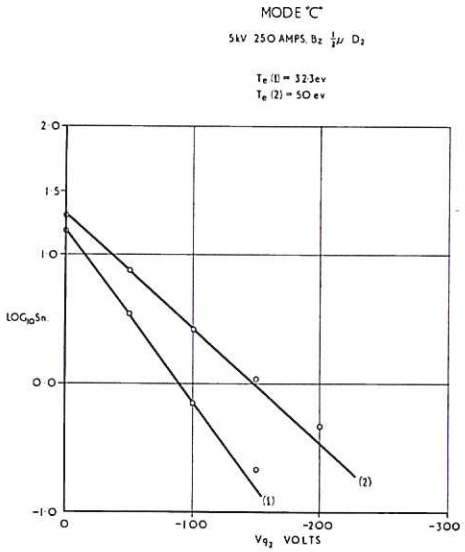

Fig. 8c

CLM - P2 Fig. 8

Logarithm of electron detector signal vers analysing grid voltage during two gates, one before and one after peak current. Results are presented for two directions of the stabilising field and for two different pressures

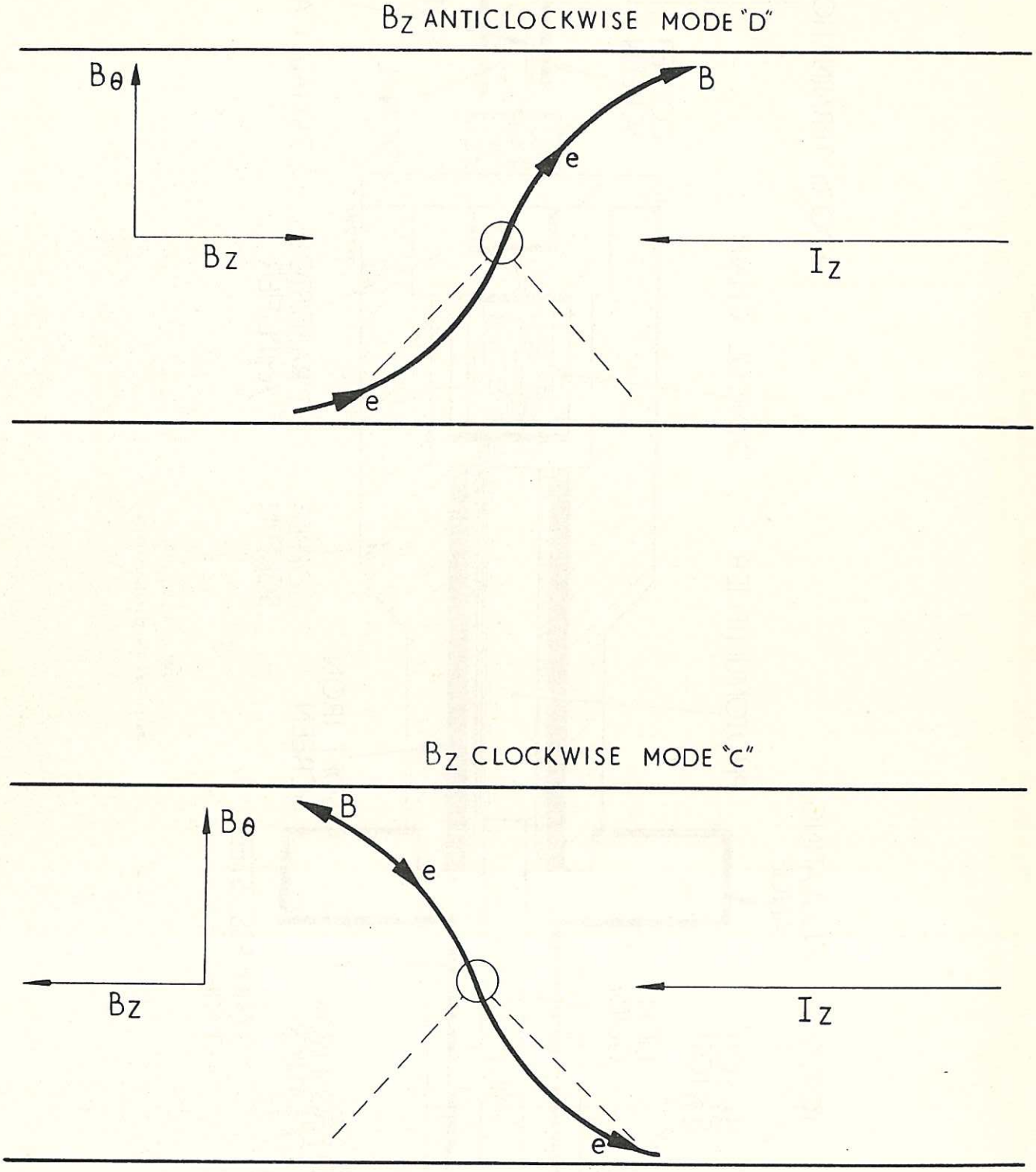

CLM - P2 Fig. 9

Magnetic field directions and electron current at the wall, viewed from the outside

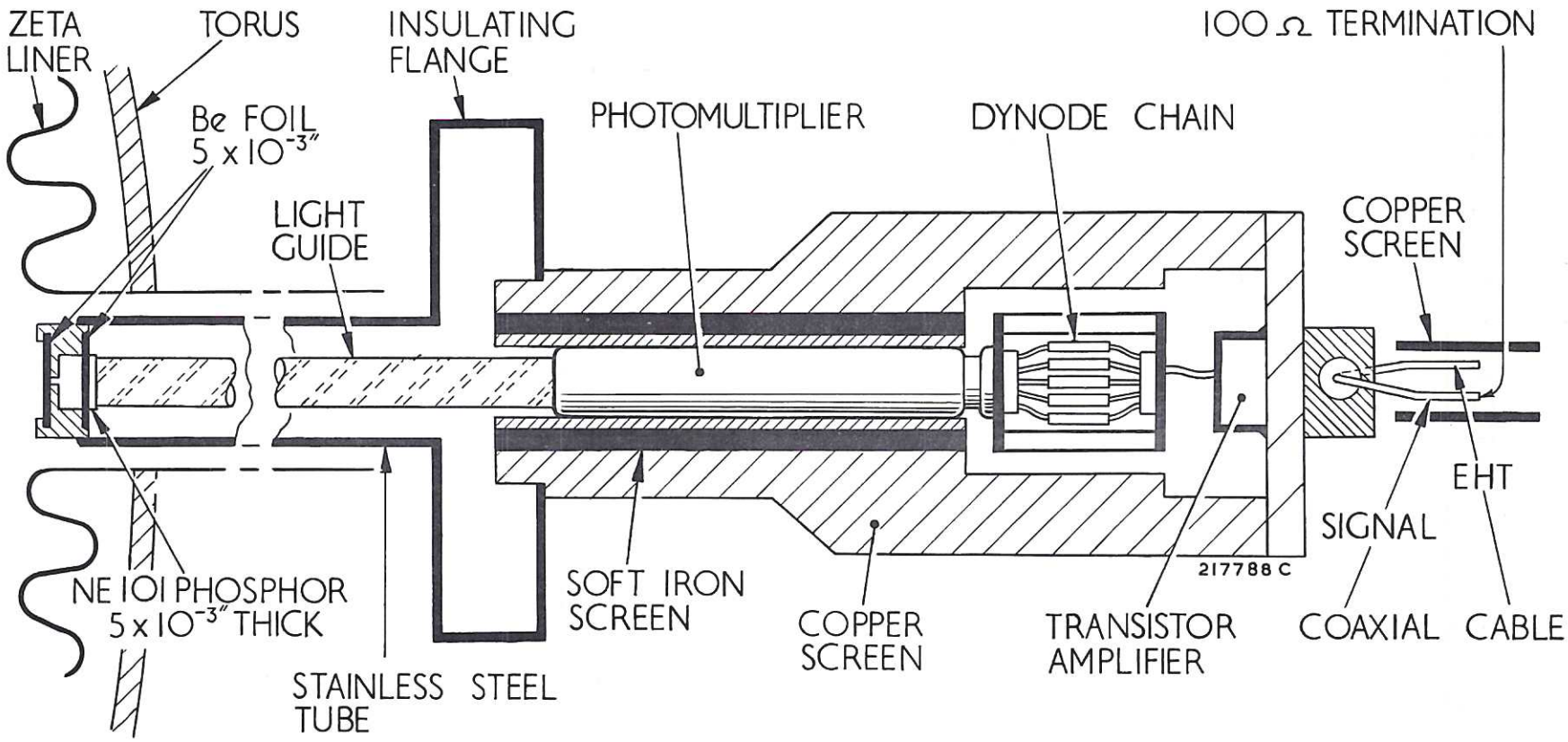

CLM - P2 Fig. 10

Soft X-ray Scintillation counter

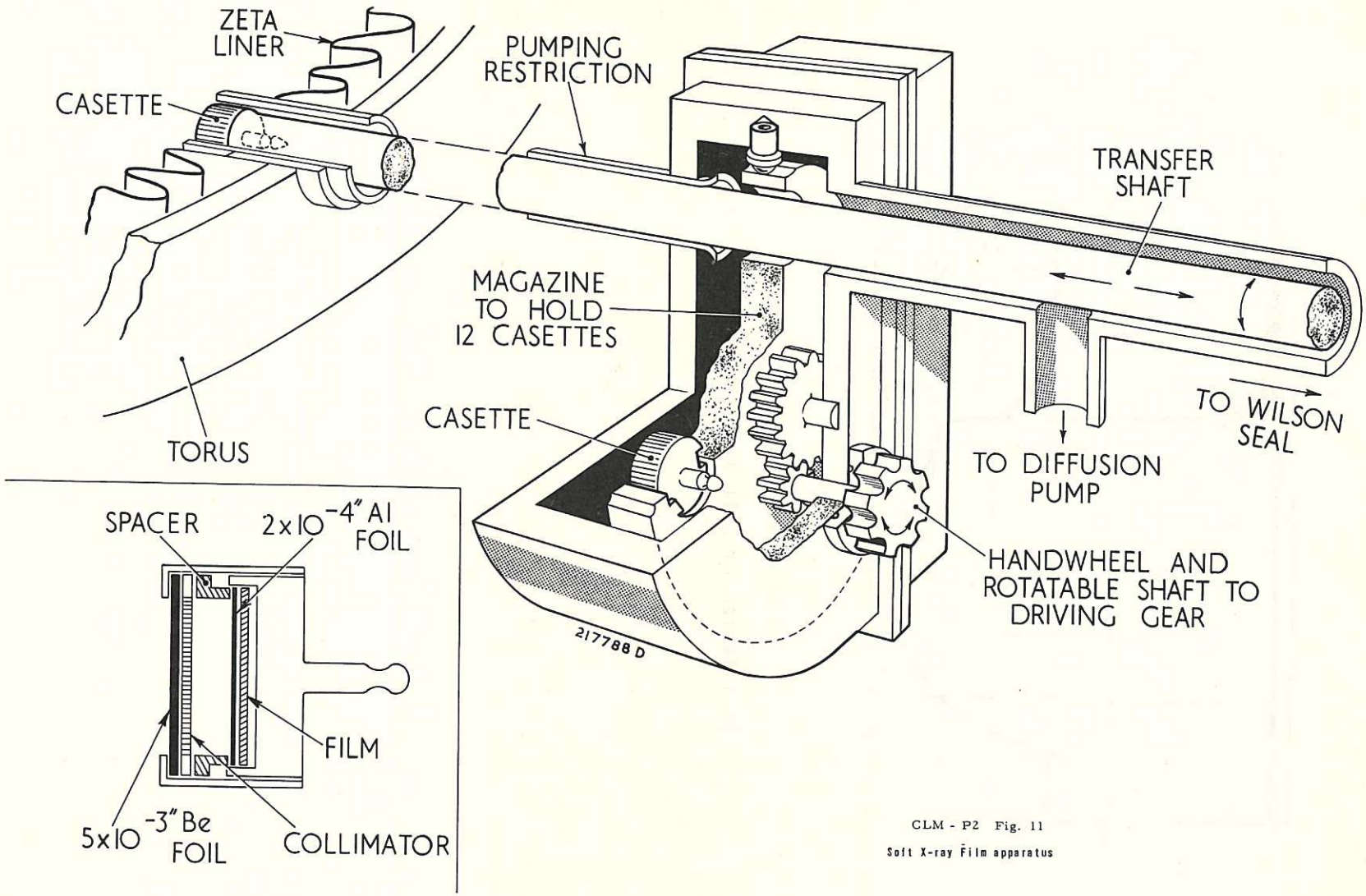

CLM - P2 Fig. 11

Soft X-ray Film apparatus

X-RAY FILM CASETTE

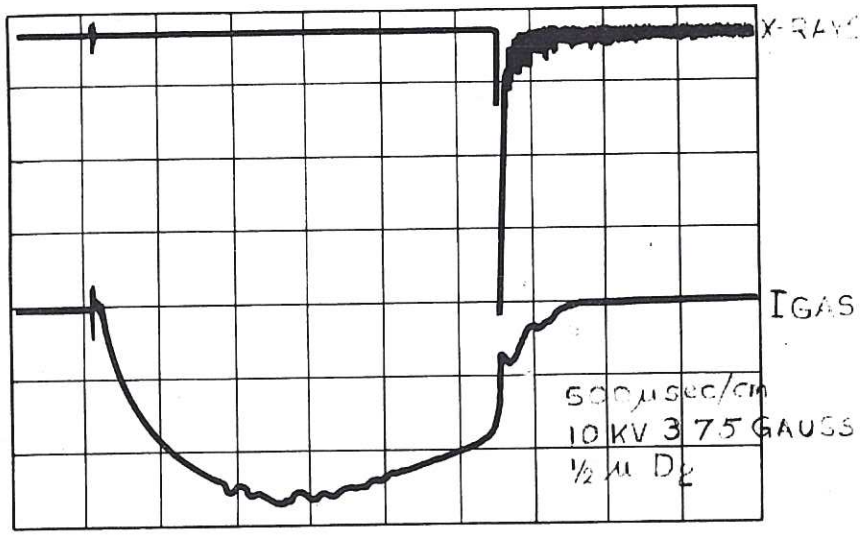

CLM - P2 Fig. 12

Oscillogram of soft X-ray emission

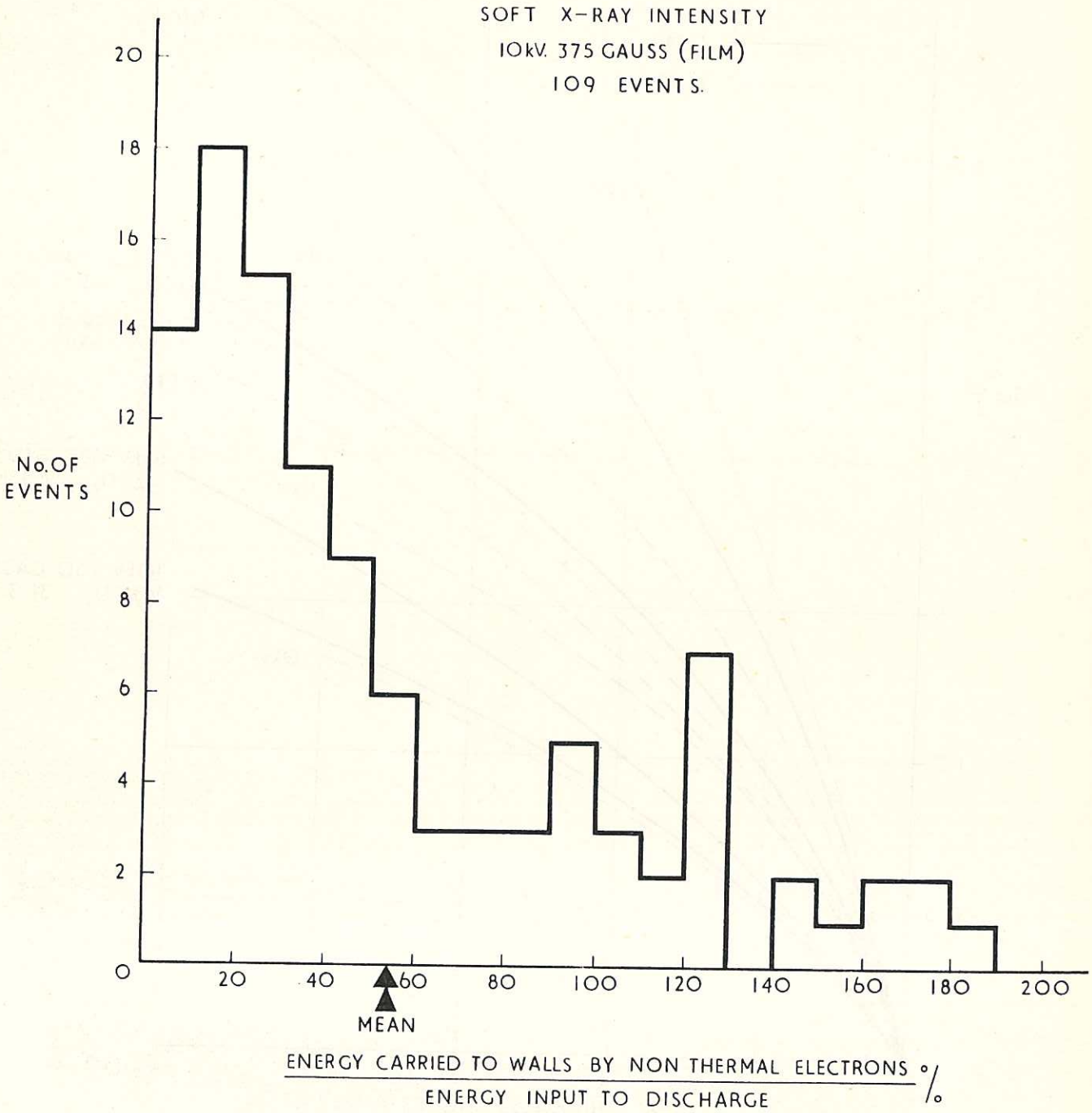

CLM - P2 Fig. 13

Histogram showing the energy lost by fast electrons as deduced from X-ray intensity measurement

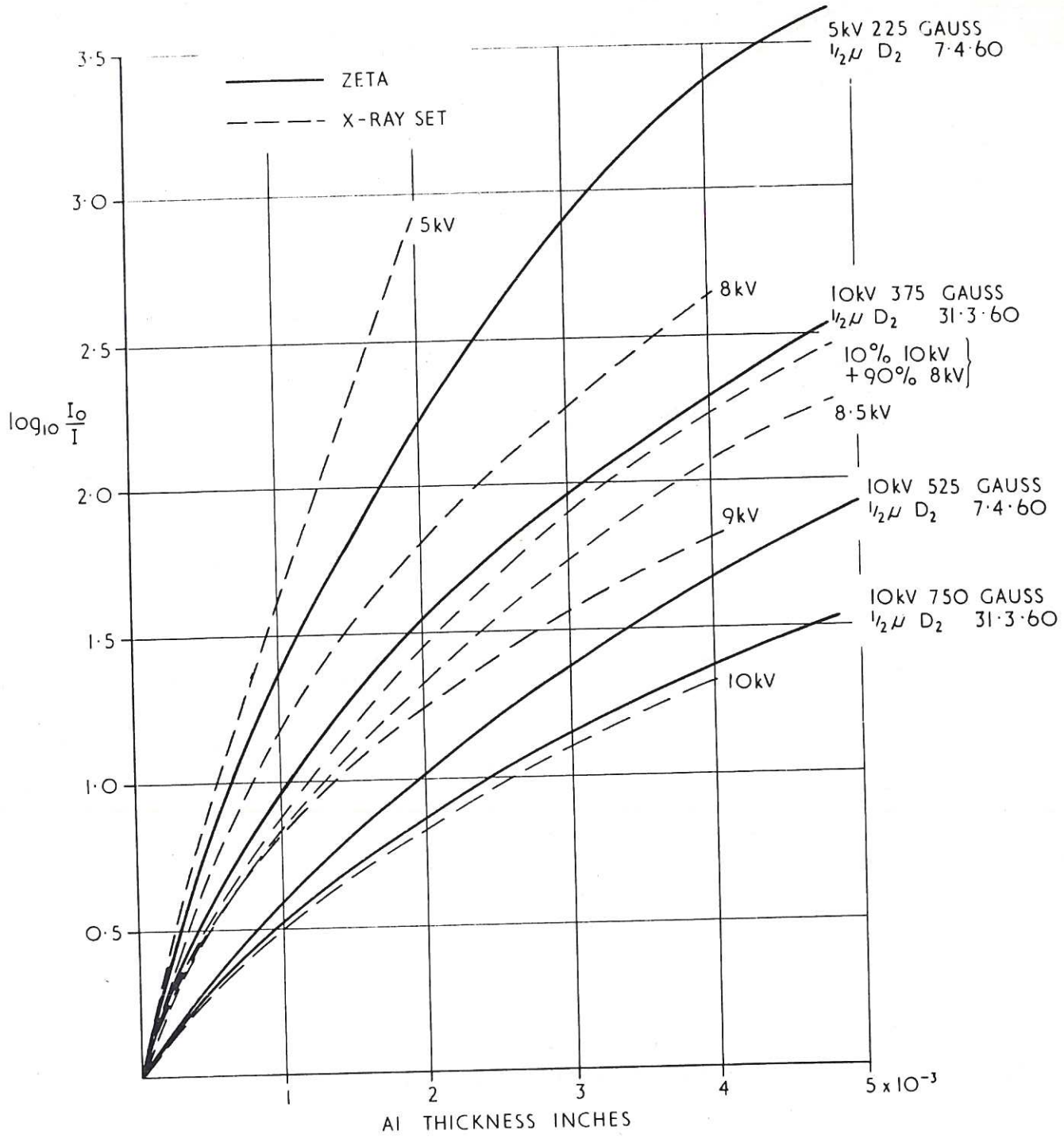

CLM 12 Fig 14

X-ray absorption curves obtained for ZETA and from an X-ray set having a monoenergetic X-ray beam

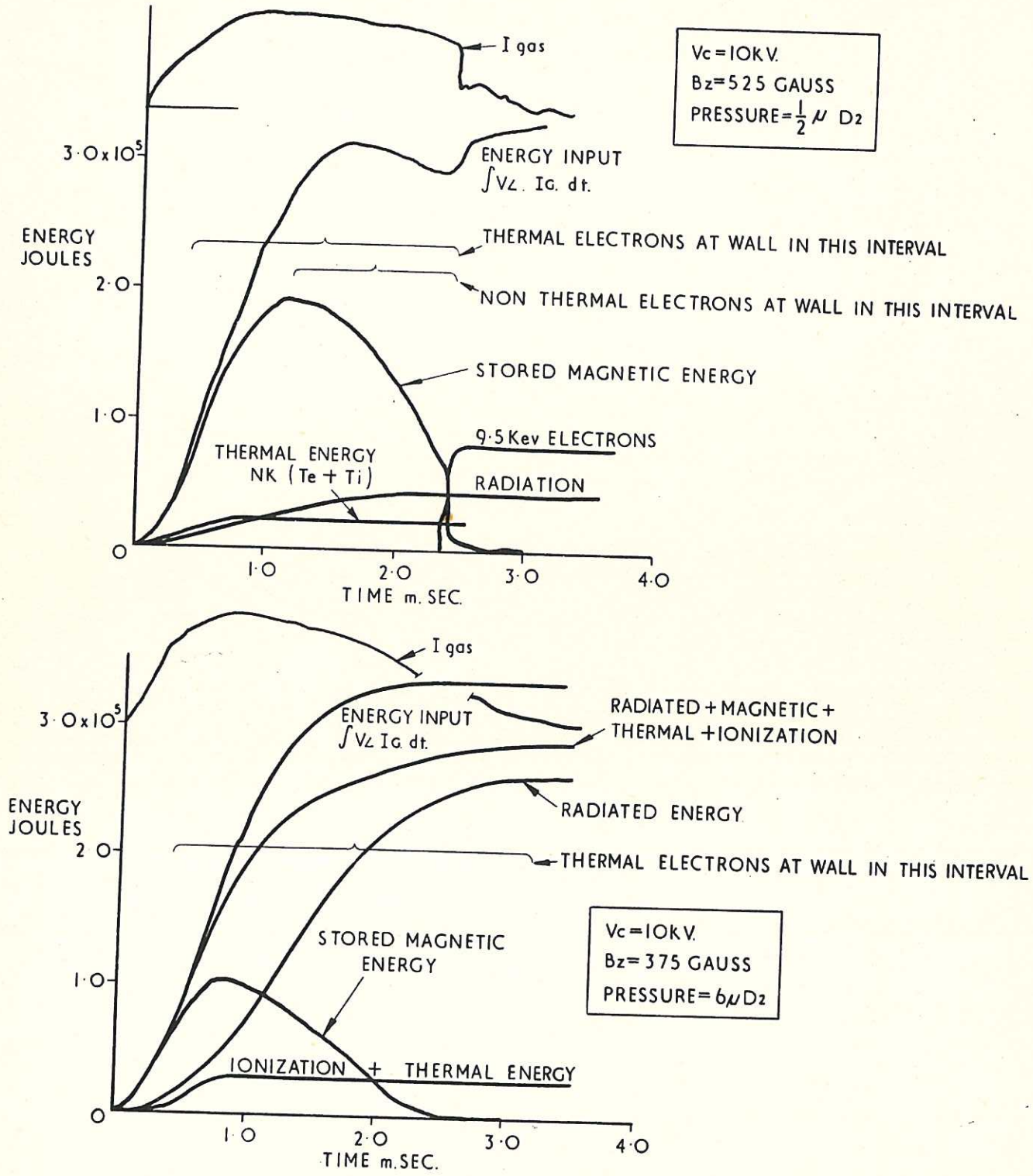

CLM - P2 Fig. 15

Summary of energy loss observations at high and low pressure